



**ANALYSIS OF SETTLEMENT OF ROCK EMBANKMENT  
WITH LATTICE FRAME REINFORCEMENT (LFR) SYSTEM**

**BY**

**MR. ISURU THARANGA DIAS RAJAKARUNA MOHOTTIGE**

**A THESIS SUBMITTED IN PARTIAL FULFILLMENT OF THE  
REQUIREMENTS FOR THE DEGREE OF MASTER OF  
SCIENCE (ENGINEERING AND TECHNOLOGY)  
SIRINDHORN INTERNATIONAL INSTITUTE OF TECHNOLOGY  
THAMMASAT UNIVERSITY  
ACADEMIC YEAR 2021  
COPYRIGHT OF THAMMASAT UNIVERSITY**

THAMMASAT UNIVERSITY  
SIRINDHORN INTERNATIONAL INSTITUTE OF TECHNOLOGY

THESIS

BY

MR. ISURU THARANGA DIAS RAJAKARUNA MOHOTTIGE

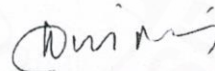
ENTITLED

ANALYSIS OF SETTLEMENT OF ROCK EMBANKMENT WITH LATTICE  
FRAME REINFORCEMENT (LFR) SYSTEM

was approved as partial fulfillment of the requirements for  
the degree of Master of Science (Engineering and Technology)

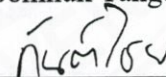
on December 7, 2021

Chairperson



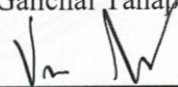
(Professor Somnuk Tangtermsirikul, D.Eng.)

Member and Advisor



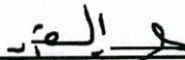
(Assistant Professor Ganchai Tanapornraweekit, Ph.D.)

Member



(Associate Professor Apiniti Jotisankasa, Ph.D.)

Member



(Qudeer Hussain, Ph.D.)

Director



(Professor Pruettha Nanakorn, D.Eng.)

Thesis Title	ANALYSIS OF SETTLEMENT OF ROCK EMBANKMENT WITH LATTICE FRAME REINFORCEMENT (LFR) SYSTEM
Author	Mr. Isuru Tharanga Dias Rajakaruna Mohottige
Degree	Master of Science (Engineering and Technology)
Faculty/University	Sirindhorn International Institute of Technology/ Thammasat University
Thesis Advisor	Assistant Professor Ganchai Tanapornraweekit, Ph.D.
Academic Years	2021

## ABSTRACT

This study investigates the behavior of the Lattice Frame Reinforcement (LFR) system under rock embankments. The LFR system is used to reduce the rate of rock embankment settlement. The LFR system contains two main components, lattice framed injected mortar polyester tube (LFR mortar tube) and polyester underlying sheet (LFR sheet). Both components are knitted together before the injection of mortar into the tubes. After the mortar was properly set, an embankment was constructed on top of the LFR system. This method significantly reduces vertical pressure on soil under the embankment. It results in lower soil settlement due to less pressure occurring under the embankment.

Two experimental embankments with the LFR system were constructed in Samut Sakhon province in Thailand for this study. The measured soil settlements under the embankments have been monitored for 30 months. Tensile tests were performed to understand the material's behavior of the LFR system. This study aims to explain the mechanism of the LFR system by applying Finite Element (FE) simulations and field measurements. The field measurement and analysis results showed that the LFR system could effectively reduce the long-term soil settlement caused by soil consolidation and self-weight of the embankment. FE Analysis shows that LFR mortar tubes behave mainly as tensile members and there is a significant effect of the grid spacing of the

LFR mortar tubes on settlement reduction. Injected mortar in the LFR system provides construction stability and supports to keep the LFR tubes in a stretched condition. Mortar has a significant effect on the LFR system due to bond contact initiated during the injection of liquid mortar. Even though the mortar has started damage since the initial stage of the embankment construction, yet damaged mortar provides stiffness enhancement to the LFR tubes. This enhancement tends to increase the stiffness of the overall LFR system. A realistic contact between damaged mortar and LFR tubes is difficult to simulate. Therefore, this study presents a simple method to simulate the stiffness of the LFR mortar tube which considers stiffness of the LFR tube together with the contribution of stiffness of mortar in between cracks which are known as tension stiffening, in the analysis.

**Keywords:** Coastal embankments, Embankment settlement, Field measurements, Finite Element Analysis, Lattice Frame Reinforcement (LFR), LFR mortar tube.

## ACKNOWLEDGEMENTS

First and foremost, the author would like to express his greatest gratitude to his advisor, Asst. Prof. Ganchai Tanapornraweekit, for his comprehensive knowledge, guidance, and encouragement throughout this study. His expertise and persistence contribute to the improvement in this study and my knowledge.

The author wishes to give his sincere appreciation towards, the chairman of the examination committee, Prof. Dr. Somnuk Tangtermsirikul, for guiding this research and providing opportunities to pursue his graduate study. Moreover, his constructive advice and suggestions in every aspect make this research interesting and provide academic enlightenment to the young researchers. The author would like to thank his committee members, Assoc. Prof. Apiniti Jotisankasa, for his insightful comments, supports, and guidance during this study, and Dr. Qudeer Hussain for his very early guidance, expertise for this research in the initial stage of the project. The author would like to acknowledge Sirindhorn International Institute of Technology, Thammasat University, for providing a full scholarship during this study time. The author wishes to thank Ashimori Industry Co., Ltd, and Teijin Frontier Co., Ltd., and Centre of Excellence in Material Science, Construction and Maintenance Technology Project, Thammasat University for providing parts of the research fund for this study.

Thanks are also extended to all the staff in student affairs and school secretaries who help me through this study time into convenient days without worrying about document works. My great appreciation is conveyed to all the technicians who helped me during my experiments with their patience and technical skills. Thanks to all students from the school of Civil Engineering and Technology who help me throughout my study time. Greatest thanks to Rajendra Prasad Bohara, Satish Paudel, Arosha Dabarera, Su Hlaing Myint, Hakas Prayuda, Suphawit Untimanon who help me to accomplish my FEM simulation works with their experiences and knowledge. Most of all, I would like to express my gratitude to my mother who support and strengthen me mentally to achieve dreams and goals in my academic life.

Mr. Isuru Tharanga Dias Rajakaruna Mohottige

## TABLE OF CONTENTS

	Page
ABSTRACT	(1)
ACKNOWLEDGEMENTS	(3)
LIST OF TABLES	(7)
LIST OF FIGURES	(8)
LIST OF SYMBOLS/ABBREVIATIONS	(11)
CHAPTER 1 INTRODUCTION	
1.1 Proposed Lattice Frame Reinforcement (LFR) system	4
1.2 Mechanism of LFR system	4
1.3 Background	6
1.4 Problem statement	7
1.5 Objectives	8
1.6 Scope	8
CHAPTER 2 REVIEW OF LITERATURE	10
2.1 Soil grain size and its contribution to soil settlement	10
2.2 Finite element analysis by PLAXIS	12
2.3 Finite Element Analysis by LS-DYNA and ANSYS	15
2.4 Types of elements in FEM	19
2.5 Applications of LFR system	22
CHAPTER 3 METHODOLOGY	25

	(5)
3.1 Experimental program	26
3.1.1 Embankment test site	26
3.1.2 Details of soil investigation	28
3.1.3 Field monitoring for embankment settlement	30
3.1.4 Field measurements of the embankment settlement	31
3.1.5 Investigation of material properties of LFR system by Lab tests	32
3.1.6 Results of laboratory tests	33
3.2 Finite element analysis of the verification model	35
3.3 Finite element simulation of the tested embankment with LFR system	38
3.3.1 Element types, sizes, boundary conditions, and contacts of FEM	42
3.3.2 Material models	44
3.3.2.1 Soil layers and embankment	45
3.3.2.2 LFR underlying sheet	46
3.3.2.3 LFR mortar tube	47
3.4. Finite element analysis cases	48
3.4.1 Case 1 – Simulation of LFR mortar tube by modeling both tube and mortar	48
3.4.2 Case 2 – Simulation of LFR mortar tube by modeling of LFR tube with tension stiffening effects	50
<b>CHAPTER 4 RESULTS AND DISCUSSION</b>	<b>53</b>
4.1 Investigation of mortar damage	53
4.2 Stress investigation of LFR system	54
4.3 Comparison of field measurements with FE results from analysis Case 1 and case 2	57
4.4 Efficiency of the LFR system	60
4.5 Rehabilitation of the rock embankment	61
<b>CHAPTER 5 CONCLUSIONS</b>	<b>63</b>

(6)

REFERENCES

65

BIOGRAPHY

68





**LIST OF TABLES**

Tables	Page
2.1 Element types used in FEM	19
2.2 Material properties of soil and pile raft	20
3.1 Material properties of LFR tube	34
3.2 Material properties of LFR sheet	34
3.3 Material properties of soils and embankment	37
3.4 Averaged element sizes	42
3.5 Contacts and types of FEM	44
3.6 Soil and embankment properties of FEM	45
3.7 General information of LFR sheet	47
3.8 Summary of material properties for LFR mortar tube in analysis case 1	49
4.1 Comparison of embankment settlements	59

## LIST OF FIGURES

Figures	Page
1.1 Rock embankment construction	2
1.2 Typical geosynthetic products used for different geotechnical Applications	3
1.3 Components of the LFR system	4
1.4 Force reduction due to larger area of the LFR system	6
1.4 Test embankment of this study with 1m × 1m and 2m × 2m LFR systems	6
2.1 Unified soil classification system	11
2.2 Settlement stages of soil	12
2.3 Maximum horizontal movement of D-walls	13
2.4 Numerical simulation performed in PLAXIS platform	13
2.5 Soil clarifications from site investigation	14
2.6 Surface settlement of soil	15
2.7 D-wall movement and distance from the wall	15
2.8 The parameters of loading process	16
2.9 Propagation of fissures in soil	16
2.10 Settlement vs pressure distribution of soil	17
2.11 The lines of equal deformations of shear at a settlement of the stamp	18
2.12 Dependence settlement from vertical loading at different eccentric	18
2.13 Settlement of the pipe	21
2.14 Stress contours of pipeline	21
2.15 Deformation contours of pipeline	22
2.16 Stress distribution of pipe	22
2.17 Application of LFR system for road construction	23
3.1 Embankment site	26
3.2 Experimental embankments	27
3.3 LFR system	27
3.4 Installation of LFR system at the test site (2m × 2m tube spacing)	28
3.5 Details of LFR mortar tube cross-section	28

3.6 Elevation data of bore logs.	29
3.7 Examples of undisturbed soil samples	30
3.8 Settlement data collecting procedure	31
3.9 Embankments with LFR systems being monitored	32
3.10 Embankment settlement with LFR systems	32
3.11 Tensile tests of LFR components	33
3.12 Tensile stress-strain relationship of the LFR tube specimens	34
3.13 Tensile stress-strain relationship of the LFR sheet specimens	35
3.14 Tested specimens	35
3.15 Soil layers and embankment details	36
3.16 Verification of the FE model without LFR system	37
3.17 Comparison of FEA results with field measurements	38
3.18 Embankment and LFR system setup	39
3.19 Studied finite element model	40
3.20 Tension stiffening effects in RC members	41
3.21 Demonstration of boundary conditions of the FEM	43
3.22 Contact types used in the FE model in this study	44
3.23 LFR underlying sheet	46
3.24 Stress strain curve of LFR sheet	47
3.25 LFR mortar tube composite	48
3.26 Stress-strain curve of LFR tube	49
3.27 LFR tube in analysis case 2	50
3.28 Proposed tension stiffening (TS) stress-strain curve to model the LFR tube by incorporating the contribution of cracked mortar	51
4.1 Damages of mortar in terms of effective plastic strain	54
4.2 Highly mortar damaged location	55
4.3 Stress plot of the LFR tube	56
4.4 Stress contour of LFR sheet	56
4.5 Plots of X- and Y- stress in LFR sheet	57
4.6 Comparison of field measurements and FE results for 1m × 1m LFR system	58
4.7 Comparison of field measurements and FE results for 2m × 2m LFR system	58
4.8 Settlement of embankment with and without LFR system	60

(10)

4.9 Contour plots of the embankment settlements

61

4.10 Rehabilitated embankment

62



**LIST OF SYMBOLS/ABBREVIATIONS**

<b>Symbols/Abbreviations</b>	<b>Terms</b>
LFR	Lattice Frame Reinforcement
TS	Tension stiffening



## **CHAPTER 1**

### **INTRODUCTION**

In general, the LFR system is used to reduce the rate of coastal rock embankment settlement. The LFR system contains two main components, one is a lattice framed injected mortar polyester tube (LFR mortar tube) and the other is a polyester underlying sheet (LFR sheet). Both components are knitted together before injection of mortar into the tubes. After the mortar is set properly, an embankment is constructed on top of the LFR system. According to previous studies conducted by several researchers, this method significantly reduces vertical pressure on soil under the embankment. Therefore, it results in lower soil settlement due to less pressure occurring under the embankment.

Embankments in civil engineering refer to compacted soil (clay or rock-based) to avoid changing the level required by the terrain, or either unacceptable change in level or detour to follow a contour. If the embankment is made of rock, it is known as a rock embankment (see Figure 1.1). In road, engineering embankments are used to make domestic roads on top of the rock embankments. Embankments are the most common type of engineering works in road construction. Sometimes embankments are constructed as barriers to control water channels. Nowadays the use of embankment has been changed. In some applications, embankments are used to shield land erosion from radical sea waves. One of the main problems associated with embankments is soil settlement due to the heavy embankment self-weight.

Settlement of soil is a serious issue that geotechnical engineers encounter during the foundation design. Different types of settlement occur in soil, an immediate settlement and a long-term time-dependent settlement are the main two types. Immediate settlement occurs in every soil type due to the applied external load, but the long-term time-dependent settlement mostly occurs in clay soil due to pore water expulsion from soil particle voids (Negahdar, A., 2016).



**Figure 1.1** Rock embankment construction. (Ashimori industries Co., Ltd.)

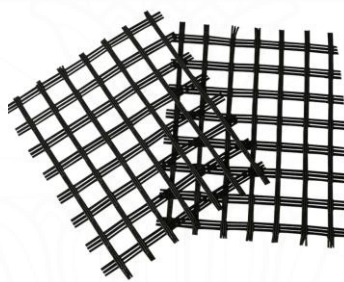
The main reason for coastal erosion is radical sea waves. Coastal erosion is a major problem that many countries are facing. The issue of coastal erosion has received considerable critical attention from all around the world. Geosynthetic products are employed for reinforcement and protection purposes in coastal areas. Geosynthetic products can be used in various forms to support subsoil with the functional requirements of the coastal areas particularly to increase the lifetime of the coastal engineering structures, i.e. rock embankments. There are many commercially available geosynthetic products such as geogrid, geonet, and geocell. They work properly when the subsoil is sufficiently strong. Therefore, based on the nature and type of coastal erosion problem for a particular location, it is important to install properly designed geosynthetic applications (A.S. Sahu, 2014).

Geonet resembles geogrid (see Figure 1.2 (a)). However, contrary to geogrids, they do not feature equivalent strength properties. In the construction industry, geonet is mainly used for drainage of liquids or exhaustion of gases. Its main function is for drainage, and when combined with geotextile they often form a geocomposite. Geonet does not act as soil reinforcement which means that the geonet does not increase the bearing capacity of the soil. Geonet is typically applied for road constructions, especially controlling soil erosion in land slope areas. On the other hand, geogrid is used to reinforce the soil underneath. Geogrid consists

(see Figure 1.2 (b)) of the sheet polymeric structure of a system of mostly perpendicular tensile longitudinal and lateral ribs that may be continuously mutually connected at the intersection, by welding, gluing, and interlacing. This configuration allows soil/rock particles to get through the geogrid's apertures. Geogrids are typically applied for road construction, especially controlling embankment erosion. Geocell is a system of interconnected surface textured perforated or smooth strips. These strips are connected by welding in order to form a honeycomb pattern as shown in Figure 1.2 (c). The system is made from a high-density polyethylene (HDPE) or polypropylene (PP). This system is mostly applied to reinforce a low-bearing subsoil, stabilize surfaces of eroded slopes, reinforce stream banks and dikes, or erect retaining walls ([www.benda-trade.cz](http://www.benda-trade.cz)).



(a) Geonet ([indiamart.com](http://indiamart.com))



(b) Geogrid ([ecogeosolution.com](http://ecogeosolution.com))



(c) Geocell ([ecogeosolution.com](http://ecogeosolution.com))

**Figure 1.2** Typical geosynthetic products used for different geotechnical applications

However, there are some common disadvantages to applying these geosynthetic products. For example, the long-term performance of geosynthetics can be chemically ultraviolet stabilized which is harmful. Obstructing geosynthetics is challenging for specific soil types such as loose soils and sandy soils in coastal areas. The carrying, handling, storage, and installation of these products must be assured by good quality control and good quality assurance.

Countries with seashores apply sea wave breakers to minimize this effect on their precious lands. Wave breakers are mainly rock embankments made of gravel. However, due to heavy loads of these rock embankments, the soil of seashores areas shows a considerable amount of settlement in a long-term



consideration. Therefore, a sustainable solution is required to solve this issue. For this reason, Lattice Frame Reinforcement (LFR) system has been proposed to use several years ago by Yoshida et al., 2006.

### 1.1 Proposed Lattice Frame Reinforcement (LFR) system

Generally, the LFR systems were applied under embankments. The system is a combination of polyester sheet (LFR sheet) and mortar-injected polyester tubes (LFR mortar tube) which are arranged in the form of lattice as shown in Figure 1.3. LFR systems for road construction were investigated by many researchers such as Okamoto et al., 2009, Okamoto et al., 2016 and Yoshida et al., 2006. However, the effects of the LFR system with embankment have not been studied for long-term soil settlement. This study aims to explore the long-term soil settlement behavior of rock embankment with the LFR system located in coastal areas.

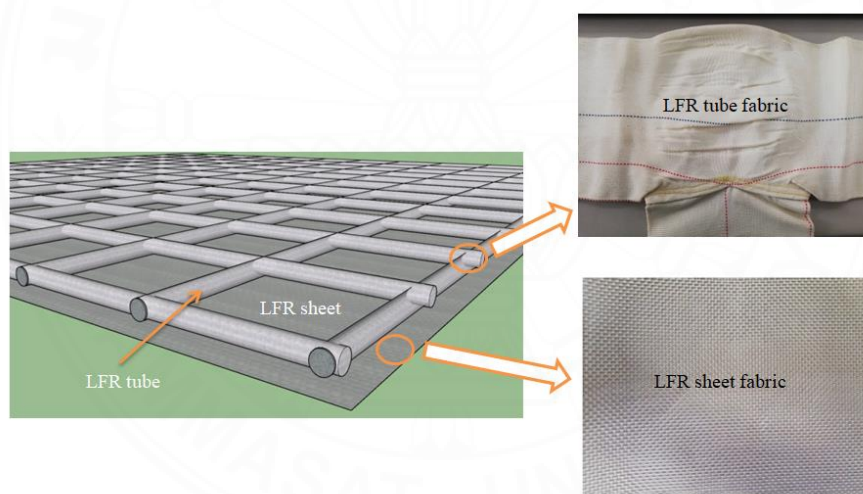


**Figure 1.3** Components of the LFR system

### 1.2 Mechanism of the LFR system

Initially, the function of the injected mortar is to maintain the circular shape and maintain the stretched nature of the LFR tubes. The LFR tubes and the underlying LFR sheets are knitted to each other to avoid any separation between these two components. However, the injected mortar is expected to provide some sorts of contribution to the LFR tube due to the bond between the inner face of the tube and the mortar inside that occurred during the injection of liquid mortar. In

addition, the self-weight of the mortar tubes makes the LFR system stands still as much as possible during the construction which results in better constructability.

The load path of the system is important to understand the mechanism of the LFR system. The vertical self-weight of the embankment is transferred horizontally to the LFR tubes and sheet via friction between the underlying sheet and surface soil. It is noted that the sheet and tubes resist tension when the sheet and tubes are in a stretch condition where this condition can be maintained via interlockings between rock-rock and rock-tube and tube-sheet. Similarly, frictional forces occur between the underlying sheet and soil surface.

Among many contacts between each component in the LFR system, the complex contact is the contact between mortar and tube. The behavior of the bond between mortar and the tubes is anticipated as follows, during the injection of the mortar into LFR tubes, a certain proportion of liquid mortar is absorbed by the tube and hardened initiating a bond contact between the mortar and the LFR tube. The mortar inside mainly contributes to the enhancement of stiffness of the composite LFR tube. Since mortar is weak in tension, therefore, the tensile strength of this composite system mainly relies on the tensile strength of the polyester tube. The rate of stiffness enhancement of the tube is not constant throughout the entire stress-strain relationship. The stiffness of the composite LFR tube is enhanced significantly during the initial stage of service (low-stress level in the LFR tube) where mortar remains intact. After mortar breaks, however, enhancement in tensile stiffness of the system by the mortar is rather low. Finally, the stiffness of the composite LFR mortar tube is at the same level as that of the standalone LFR tube. It is noted that in addition to the breaking of mortar, slippage at certain interfaces of the mortar and LFR tube also degrades the level of stiffness enhancement of this composite system. Due to the larger area of the LFR system than the embankment base, the magnitude of the force on the soil surface is reduced significantly. Therefore, the settlement of embankment is lowers compared to the embankment without the LFR system. The concept is shown in Figure 1.4.

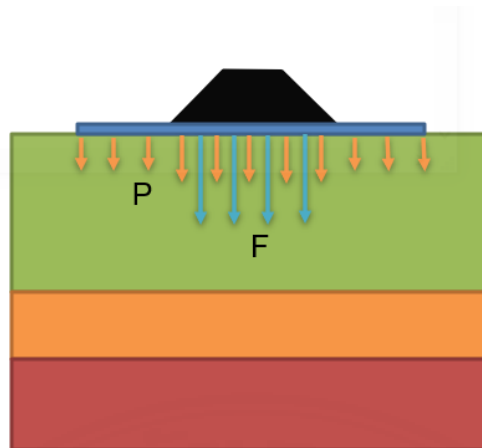


**Figure 1.4** Force reduction due to larger area of the LFR system

### 1.3 Background

In this research, two rock embankments that were constructed in seashore areas of Samut Sakhon province were considered as the case studies. The site is located at a seashore area where soil surface and seawater levels are assumed at the same level. The LFR system is applied under the embankment. Field settlement measurements were monitored from these embankments (see Figure 1.5). These embankments were constructed with the LFR system of two different LFR tube spacings ( $1\text{m} \times 1\text{m}$  and  $2\text{m} \times 2\text{m}$ ). There are different types of soil in the seashores of Thailand, e.g. clay, silty and sandy soils as mentioned by Saengsupavanich, C (2009). These soil types undergo different levels of soil settlement.



**Figure 1.5** Test embankments of this study with  $1\text{m} \times 1\text{m}$  and  $2\text{m} \times 2\text{m}$  LFR systems

Coastal erosion has been a serious issue in Thailand for many years according to the Ministry of Natural Resource and Environment of Thailand, Department of Mineral Resource. Saengsupavanich, C (2009) investigated how Thailand applied an integrated approach to tackle erosion problems to mitigate coastal erosion.

There are two types of soil settlement. One is the immediate settlement, and another is the long-term settlement. The total settlement of any structure is the combination of immediate and long-term settlements. Although studies were done by Okamoto et al., 2009, Okamoto et al., 2016 and Yoshida et al., 2006 in which the benefits of using the LFR system to reduce settlement were recognized, additional research need to be systematically investigated on the effects of the long-term settlement of the LFR system under embankments for the benefits of the design of the system. In addition, the LFR system has not been studied with different tube configurations such as different spacing of the LFR mortar tubes.

#### **1.4 Problem statement**

Rock embankments were used to reduce the coastal erosion in some areas in the Gulf of Thailand. Thailand has widely adopted mangroves forests and bamboo walls against harmful sea waves for decades. In recent years, rock embankments have been adopted as a more durable and long-term solution than mangroves or bamboo walls. Despite its long-term durability success, many rock embankments have a major problem which is settlement due to its large self-weight. Hence seashore soils undergo settlement problems, and it is necessary to introduce a method to reduce the settlement of the embankments with longer service life.

The main purposes of this study are to develop the LFR system, which is compatible to apply with rock embankments and to understand the mechanism of the LFR system under the embankments. The LFR system facilitates slowing down the future settlement of the embankment to achieve the maximum service time. The large self-weight of rock embankments cannot be avoided since the height of the rock embankments is crucial to keep their active status and to protect shores from sea waves. Sinking of coastal rock embankments due to soil settlement causes

disfunction of the embankment. Therefore, it is crucial to minimize possible settlements.

### 1.5 Objectives

The main objectives of this research are to investigate the long-term behavior and mechanism of the tested LFR system under rock embankments located in Thailand and to develop a reliable Finite Element Model to investigate the effectiveness of the LFR system to reduce embankment settlement. To achieve the mentioned objectives, this study is sectioned as follows.

- Finite element models are developed with the LFR system of 1m x 1m and 2m x 2m arrangements to investigate the soil settlement. Therefore, laboratory test results and soil investigation reports are used for material properties.
- Two different approaches are considered in the Finite Element Analysis. The first case is the composite LFR mortar tube which contains mortar. The second case is the model with the LFR tube without mortar. In this case, a tension stiffening concept is considered to enhance the stiffness of the LFR tube.
- Mortar damage in the LFR system will be investigated using FEM.
- Finally, the finalized FEM can be used to customize the design parameters to optimize the system according to different requirements that may arise in the future

### 1.6 Scopes

Several limitations were considered in this study to reduce the complexity of the FEM. such as,

- Field test data are gathered from the site located in Samut Sakhon, Thailand.
- Two types of LFR systems which are 1m × 1m and 2m × 2m of mortar tube spacing are considered.
- Settlement within the embankment is considered to be negligible.

- The striking effects of sea waves on surfaces of embankments are ignored in the simulation.



## CHAPTER 2

### REVIEW OF LITERATURE

#### 2.1 Soil grain size and its contribution to soil settlement

Embankments settle due to weak soil located under embankments. The soil is present as a combination of various sizes of soil particles. Due to different sizes, soil particles show different characteristics. Mainly rocks, sand, silt, and clay are considered as the main types of soil. The rocks can be classified into three main categories such as igneous, sedimentary, and metamorphic (Geoffrey M. 2014). Soils are formed by the chemical and mechanical weathering of rocks for many years with certain environmental conditions. Based on the size of the soil particles, soil can be classified as gravel, sand, silt, and clay. Size ranges of 76mm – 4.75mm are considered as gravel, 4.75mm – 0.075mm as sand and fines, while silt and clay have sizes below 0.075mm.

Different classification standards (see Figure 2.1) propose different particle sizes as the limits of the categorizations. Among them, the unified classification system is considered for geotechnical engineering. Because of the broad scheme of classification, categorization is based on the gradation of size and the plasticity of the soil.

A study of deep excavation in the Bangkok MRT project in 2013 by Likitlersuang, S. (2013) found that there was a huge river deposit in the central plane region known as the Chao Praya delta. This delta consisted of a broad basin filled with sedimentary soils and a thick, soft to very soft clay layer deposited on the top. Soil reports of the site showed a presence of sandy and clay soils. Sandy soil undergoes sudden immediate (elastic) settlement while clay soil is affected by primary consolidation and secondary consolidation (creep) settlements.

Criteria for assigning group symbols				Group symbol	
Coarse-grained soils More than 50% of coarse fraction retained on No. 4 sieve	Gravels	Clean Gravels	$C_u \geq 4$ and $1 \leq C_c \leq 3^c$	GW	
	More than 50% of coarse fraction retained on No. 4 sieve	Less than 5% fines <sup>a</sup>	$C_u < 4$ and/or $1 > C_c > 3^c$	GP	
		Gravels with Fines	$PI < 4$ or plots below "A" line (Figure 5.3)	GM	
	Sands	More than 12% fines <sup>a,d</sup>	$PI > 7$ and plots on or above "A" line (Figure 5.3)	GC	
		50% or more of coarse fraction passes No. 4 sieve	Clean Sands	$C_u \geq 6$ and $1 \leq C_c \leq 3^c$	SW
			Less than 5% fines <sup>b</sup>	$C_u < 6$ and/or $1 > C_c > 3^c$	SP
Sands with Fines		$PI < 4$ or plots below "A" line (Figure 5.3)	SM		
	More than 12% fines <sup>b,d</sup>	$PI > 7$ and plots on or above "A" line (Figure 5.3)	SC		
Fine-grained soils 50% or more passes No. 200 sieve	Silts and clays Liquid limit less than 50	Inorganic	$PI > 7$ and plots on or above "A" line (Figure 5.3) <sup>e</sup>	CL	
		Organic	$PI < 4$ or plots below "A" line (Figure 5.3) <sup>e</sup>	ML	
	Silts and clays Liquid limit 50 or more	Inorganic	Liquid limit — oven dried	Liquid limit — oven dried	CH
			Liquid limit — not dried	Liquid limit — not dried	
		Organic	$PI$ plots on or above "A" line (Figure 5.3)	$PI$ plots on or above "A" line (Figure 5.3)	MH
			$PI$ plots below "A" line (Figure 5.3)	Liquid limit — oven dried	Liquid limit — oven dried
Highly Organic Soils	Primarily organic matter, dark in color, and organic odor	Liquid limit — not dried	Liquid limit — not dried	Pt	
		$< 0.75$ ; see Figure 5.3; OL zone	$< 0.75$ ; see Figure 5.3; OH zone		

<sup>a</sup>Gravels with 5 to 12% fine require dual symbols: GW-GM, GW-GC, GP-GM, GP-GC.

<sup>b</sup>Sands with 5 to 12% fines require dual symbols: SW-SM, SW-SC, SP-SM, SP-SC.

$$C_u = \frac{D_{60}}{D_{10}}; C_c = \frac{(D_{30})^2}{D_{60} \times D_{10}}$$

<sup>d</sup>If  $4 \leq PI \leq 7$  and plots in the hatched area in Figure 5.3, use dual symbol GC-GM or SC-SM.

<sup>e</sup>If  $4 \leq PI \leq 7$  and plots in the hatched area in Figure 5.3, use dual symbol CL-ML.

**Figure 2.1** Unified soil classification system [ Das, Braja M., 2006,)

Another case study of Sukhumvit MRT Station in 2018 conducted by Likitlersuang, S. (2018) characterized the Bangkok soil layers using the data from various locations across Bangkok. The study separated soil as made ground (MG), Bangkok soft clay (BSC), stiff clay (SC), clayey sand (CS), and hard clay (HC). The study also determined the small strain stiffness characteristics for Bangkok clay focusing on two parameters, small strain shear modulus and reference shear strain based on laboratory testings. The soil may result in an immediate settlement, primary consolidation, and secondary consolidation settlement due to the presence of the mentioned soil types above. Immediate settlement may occur immediately after the embankment was constructed and continued up to a few days (see Figure 2.2).



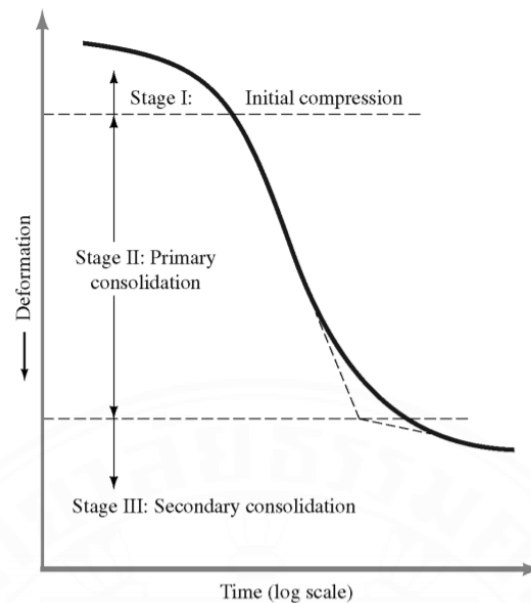


**Figure 2.2** Settlement stages of soil [Likitlersuang, S. (2013)]

Primary consolidation starts at the end of the immediate settlement and continues up to the beginning of the secondary consolidation settlement of the soil. At first, water retains inside the soil pores where this porewater is stressed under loading, while the soil particles are unstressed. In the consolidation process, porewater drains out from the soil pores eventually, which leads soil particles to start stressing out eventually from the embankment load. At this stage, the primary consolidation starts, and the secondary consolidation start once all the pore water drains out because in the secondary consolidation drained soil particles are rearranged and then reduces voids among soil particles.

## 2.2 Finite element analysis by PLAXIS

In 2013, a 2D plane strain approach by PLAXIS was used to model the excavation of Sukhumvit station by Likitlersuang, S. (2013). Only half of the station box was modeled due to symmetry. Figure 2.3 shows the maximum horizontal movement of the D-wall after stage 4 excavation. Seven layers of the soil profile were adopted. Thoughtfully, there were four soil models i.e., Mohr–Column model (MCM), soft soil model (SSM), hardening soil model (HSM), and hardening soil model with small-strain stiffness (HSS), which were used to evaluate their

performances in the deep excavation modeling. Soil layers were modeled using 15 node elements and structural components such as walls, platform slabs, base slabs, columns, and piles were modeled using non-volume plate elements (see Figure 2.4). In the HSM analysis, the lateral wall movement and the ground surface settlement prediction revealed almost identical wall movement profiles and surface settlement envelopes of the model.



**Figure 2.3** Maximum horizontal movement of D-walls [Likitlersuang, S. (2013)]

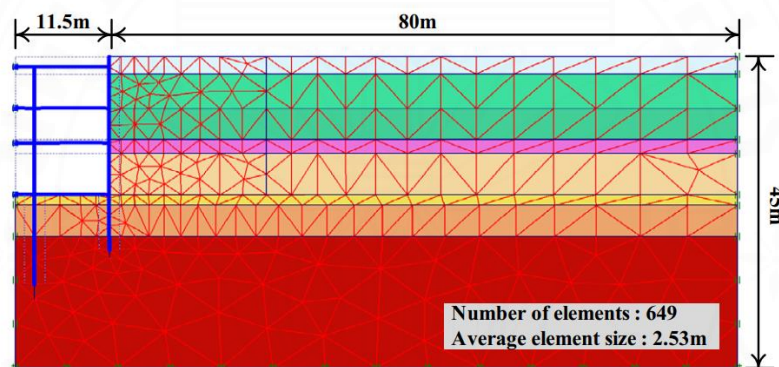


**Figure 2.4** Numerical simulation performed in PLAXIS platform [Likitlersuang, S. (2013)]

For investigation purposes, (see Figure 2.5) the effects of the initial pore water pressure condition were assigned in two methods to the finite element model. Therefore, two analyses were conducted, the first method was drawdown pore water pressure profile, while the second method was by assuming a hydrostatic pore water pressure profile. The groundwater level was below 2m from the surface. Hardening soil models (HSM) were developed under the framework of the theory of plasticity. The total strain was calculated using a stress-dependent stiffness, hence, the stiffness was different for the loading and unloading/reloading mechanisms. The strain hardening was assumed to be isotropic, depending on plastic shear and volumetric strain.

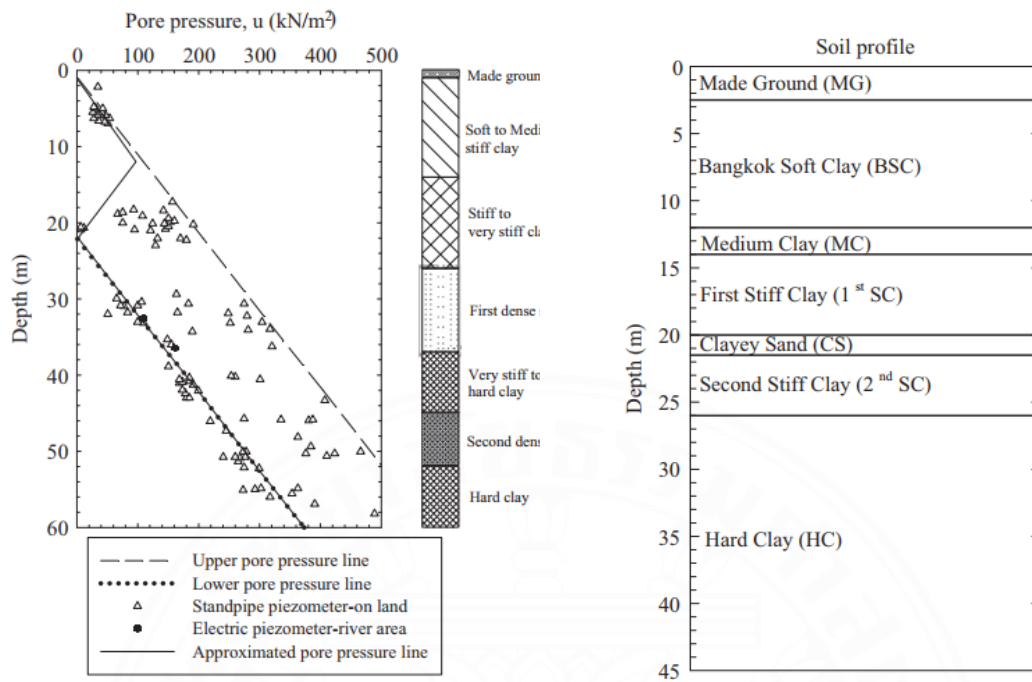


**Figure 2.5** Soil clarifications from site investigation [Likitlersuang, S.(2013)]

Lateral wall movements and ground surface settlement were obtained from a higher degree of sophistication of constitutive models in the following variety of soil models. Comparisons of finite element prediction from drawdown and hydrostatic cases are shown in Figures 2.6 and 2.7. Among the results of models of the maximum lateral wall movement, and the maximum surface settlement, the case of hydrostatic predictions was about two times higher than the corresponding field measurements. However, the drawdown case provided reasonable agreements for peak values. Finally, it can be stated that analysis and numerical methods were employed for a better prediction of the ground movements according to the study conducted by Likitlersuang, S.(2013).

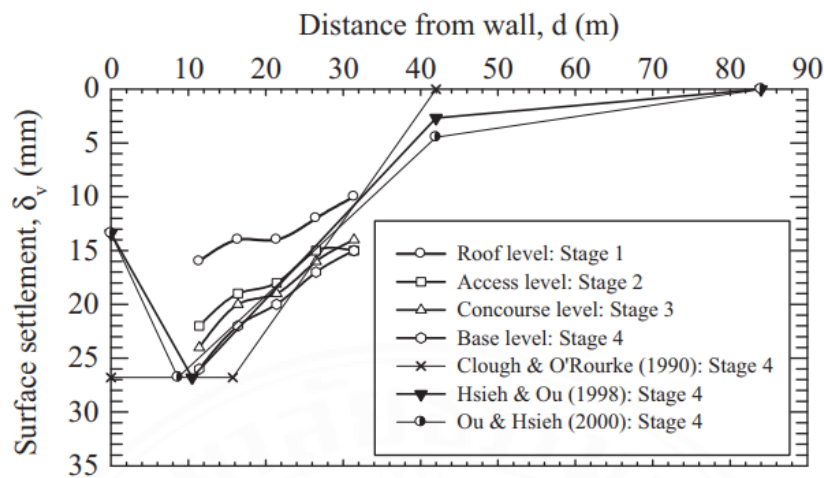


**Figure 2.6** Surface settlements of soil [Likitlersuang, S.(2013)]

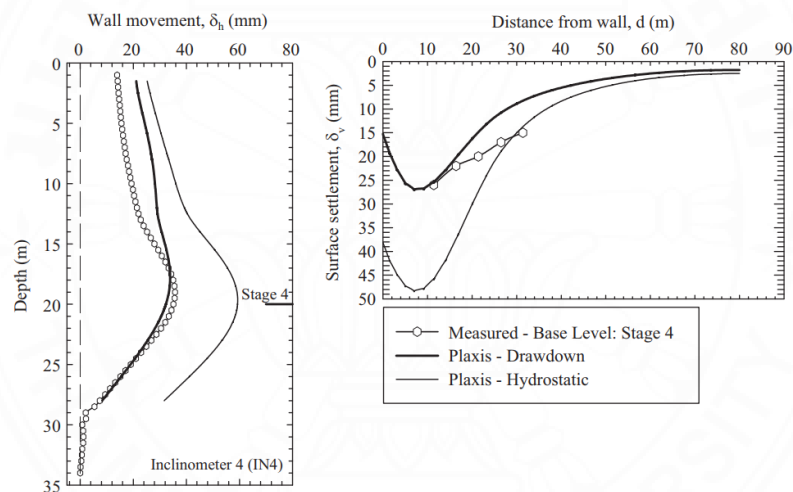


**Figure 2.7** D-wall movement and distance from the wall [Likitlersuang, S. (2013)]

### 2.3 Finite element analysis by LS-DYNA and ANSYS

A study conducted in 2008 by G.G. Boldyrev, A. (2008) explored the experimental and numerical behavior of sand deformation based on a rigid stamp which was loaded centrally and eccentrically. The problem was solved by using ANSYS and LS-DYNA finite element software. Drucker Prager soil model was used with Arbitrary Lagrangian-Eulerian (ALE) method. Also, this method can solve large deformations in sandy soil, for example when the soil loses its stability.

A model was created according to laboratory sample size, then simulated to verify the deformation process. Material parameters were given to the FE model, parameters of the loading process are shown in Figure 2.8.  $P_1$ ,  $P_2$ ,  $P_3$  are side pressures assigned as a function of time.

Test considered indenter of a steel plate with the sizes of  $0.4\text{m} \times 0.3\text{m} \times 0.1\text{m}$  in the layer of sand with the sizes of  $3\text{m} \times 3\text{m} \times 2.5\text{m}$ . During the loading process, loading on a plate and the vertical displacement of the sandy ground surface in longitudinal and cross-sections were recorded. Specimens were loaded by concentric and eccentric loadings. Measurements of the settlement were obtained using four LVDTs with an accuracy of  $0.01\text{m}$ . Hydraulic jack was set to apply the loads for the tests (see Figure 2.9).

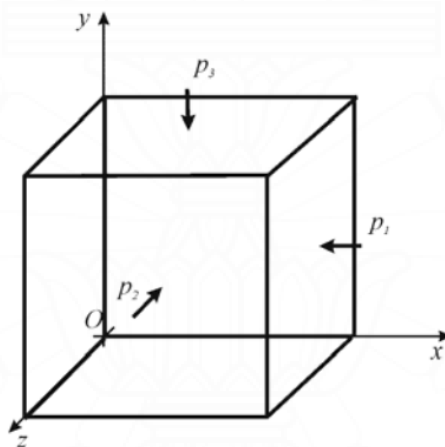


**Figure 2.8** The Parameters of loading process [G.G. Boldyrev, A. (2008)]



**Figure 2.9** Propagation of fissures in soil [G.G. Boldyrev, A. (2008)]

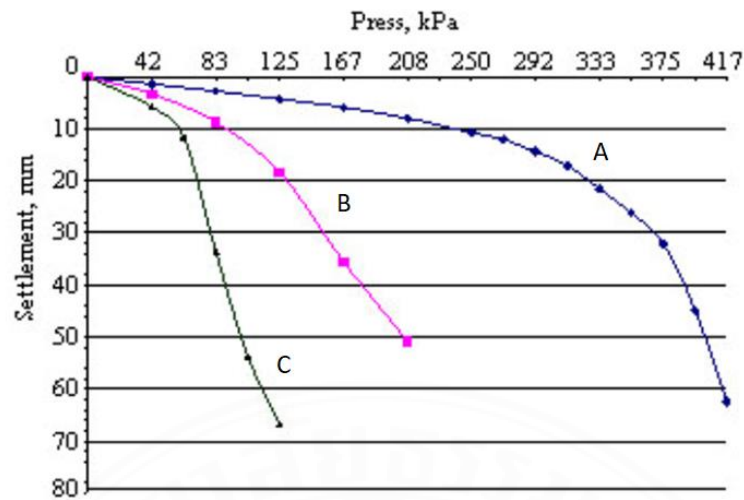


**Figure 2.10** Settlement vs pressure distribution of soil (A – central, B – eccentric of 0.05m and, C – eccentric of 0.1m) [G.G. Boldyrev, A. (2008).]

The sand failure was observed only in the specimen that was loaded at the center (case A). Case B and C showed loss of stability of the sandy soil forming a sharp settlement at the stamp (see Figure 2.10). The size of the bulges in the sand surface decreased with the increase of the eccentric load. Bulging of the ground surface adjacent to the stamp was unilateral. Formed fissures were propagated in a radial direction to the rectangular stamp. FEM modeling was carried out to determine the maximum load on the stamp implantation in sandy soil. FEA using ANSYS was performed in this study.

The analysis results showed that high shear stress affected the corner areas of the stamp and extended downwards and aside (see Figure 2.10). The maximum shear displacement was limited within the narrow region at the stamp. Incremental loading supported to develop a shear strip in which edges were displaced at the right under the stamp to the direction of the free surface of the sandy basis. The most intensive expansion of sand was observed in the direction of development of the maximum shear deformation. Deformations are shown in Figure 2.11.

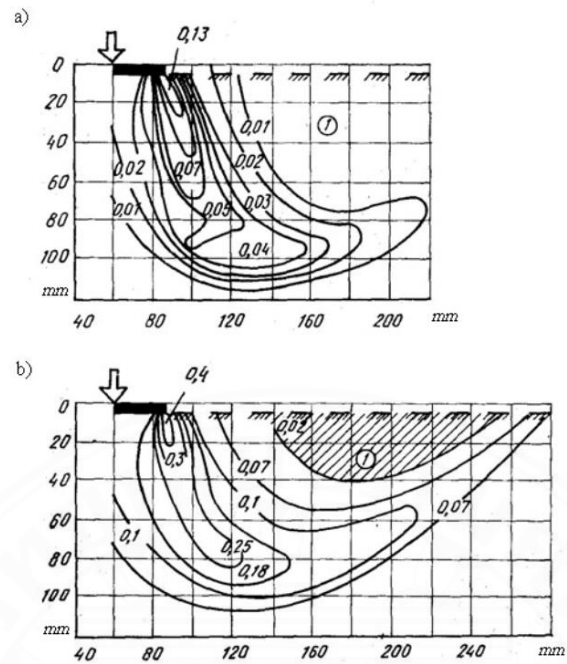


**Figure 2.11** The lines of equal deformations of shear at a settlement of the stamp, equal: a - near to a maximum load; b- behind a maximum load [G.G. Boldyrev, A. (2008)]

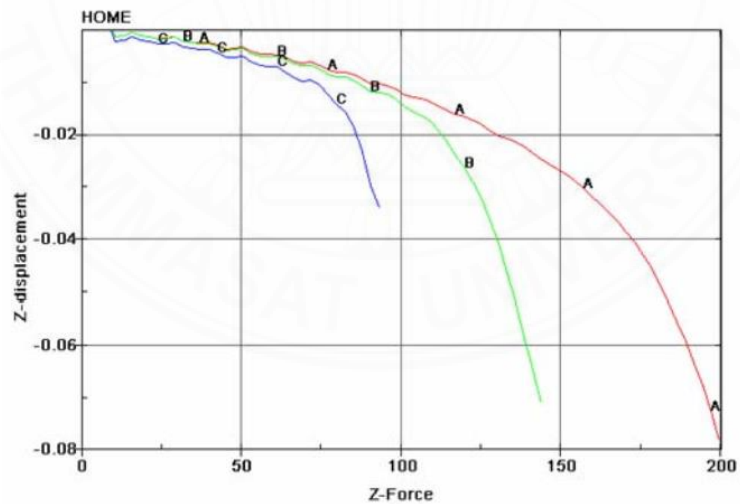


**Figure 2.12** Dependence settlement from vertical loading at different eccentric: A- central loading; B - eccentric 0.05 m; C - eccentric 0.1 [G.G. Boldyrev, A. (2008)]

A similar character of the sandy basis deformation was obtained from the numerical analysis as well. Vertical displacement at the location A, B, C of the plates is shown in Figure 2.12.

Localization of deformations as shear strips formed at large soil deformations is one of the main features of stability loss of the base foundations. Another feature of stability loss is the continuous change of deformation of the basis at its loading. The complex behavior of the bases during their stability loss causes certain difficulties in the numerical modeling of this process.

#### 2.4 Types of elements in FEM

In 2016, Gadpande, R.R. (2016) investigated the behavior of piled raft supported identical piles using FE software, ANSYS. Interactions between pile raft and soil were taken into consideration. Piles were loaded vertically where the base of the raft was treated as rough contact with soil.

**Table 2.1** Element types used in FEM [Gadpande, R.R. (2016)]

Component	Element Type
Pile	Brick-8 node-Solid 45
Raft	Brick-8 node-Solid 45
Soil	Brick-8 node-Solid 45
Contact	Contact-3D-surface to surface-Cont 174
Target	Target 170

Elements used in the FE modeling is SOLID 45 (8-noded brick element) (see Table 2.1). The analysis was performed for the raft of  $16\text{m} \times 16\text{m}$  in which the piles are  $0.4\text{m} \times 0.4\text{m}$  in cross-section. The pile was 12m in length. The structure was symmetrical; therefore, one-fourth of the piled raft was modeled. The area of soil was taken as double of the raft area whilst the depth of soil was taken as twice the raft width. Properties of soil and pile raft were considered as in Table 2.2



**Table 2.2** Material properties of soil and pile raft [Gadpande, R.R. (2016)]

Soil modulus, $E_s$ (kN/m <sup>2</sup> )	50000
Poisson's ratio of soil, $\mu_s$	0.45
Soil Cohesion, $c$ (kN/m <sup>2</sup> )	50
Soil angle of friction, $\phi$ (degree)	0
Soil dilatancy angle, $\varphi$ (degree)	0
Raft modulus, $E_r$ (kN/m <sup>2</sup> )	$2 \times 10^7$
Poisson's ratio of the raft, $\mu_r$	0.3
Raft thickness, $t_r$ (m)	1

Incremental loads were placed on the raft top to analyze the settlement of each load and the results were recorded for raft settlement. Finally, it was concluded that the settlement can be reduced by using a pile raft foundation dramatically. It was identified that nearly 60% of the soil settlement can be reduced by providing piled raft foundation system. The study found that a rough raft base may affect the vertical movement of the pile significantly. The lateral resistance of soils and piles affected the vertical movement of the raft significantly. This soil had more clay nature than normal soil in the Kandala area in India as mentioned in the study conducted by Gadpande, R.R. (2016).

P.Burkov (2014) focused on the Russian gas network's faces on difficult climate conditions that have negative aspects on gas pipeline operations and their life consistency for risk of ecological or technical disasters. The forces that were not considered in the specifications can cause significant deviations from the strength and stress deformed state (SDS) of gas pipelines. When the long-term settlement occurred in soil, pipes and their locations of the joint could be seriously damaged leading to gas exploding disasters (see Figure 2.13).

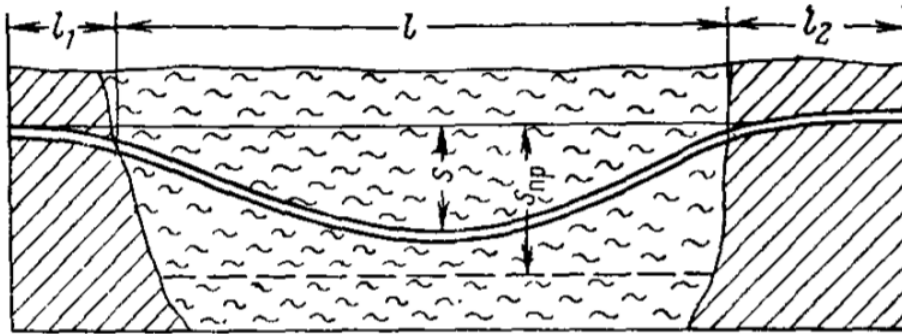


**Figure 2.13** Settlement of the pipe [Burkov, PV (2014)]

ANSYS software was used by P.Burkov (2014) for the analysis of stresses caused by the ground settlement to determine the stresses in the pipe (see Figure 2.14). The distributed load was caused by the weight of the pipe with insulation, the gas, and the pressure of overlying soil. The deformation of the pipe is shown in Figure 2.15.

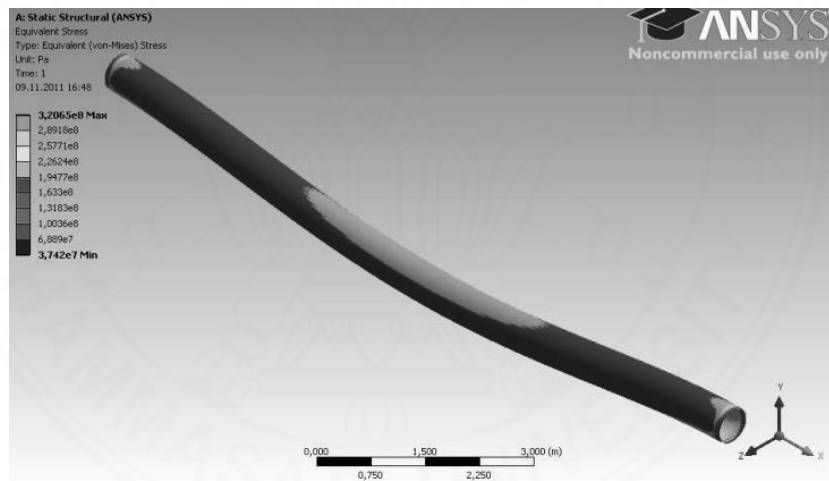


**Figure 2.14** Stress contours of pipeline [Burkov, PV (2014)]



**Figure 2.15** Deformation contours of pipeline [Burkov, PV (2014)]

Finally, the study found that changing the stress values in the pipe, which happened during the pipeline settlement, can decrease its safety level. Moreover, the intensity of stress was varied according to the length of the pipe. Higher stress levels were found in the areas where the pipeline transitioned from loose soil to hard soils (see Figure 2.16).

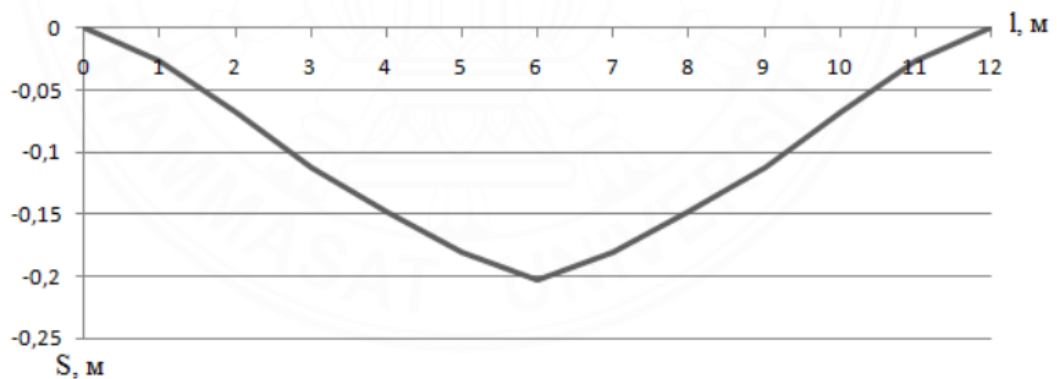


**Figure 2.16** Stress distribution of pipe (S) lengthwise (l) in the pipeline section [Burkov, PV (2014)]

## 2.5 Application of LFR system

In geotechnical engineering, settlement is defined as the vertical movement of a certain point of ground due to changes of stresses within the soil [L. Zhang et al. (2010)]. Different types of soil may undergo different amounts of settlements

depending on the bearing capacity of the soils. This settlement phenomenon causes problems for many engineering structures/applications. Lattice Frame Reinforcement (LFR) was introduced on several occasions by Okamoto M. (2009) (see Figure 2.17).

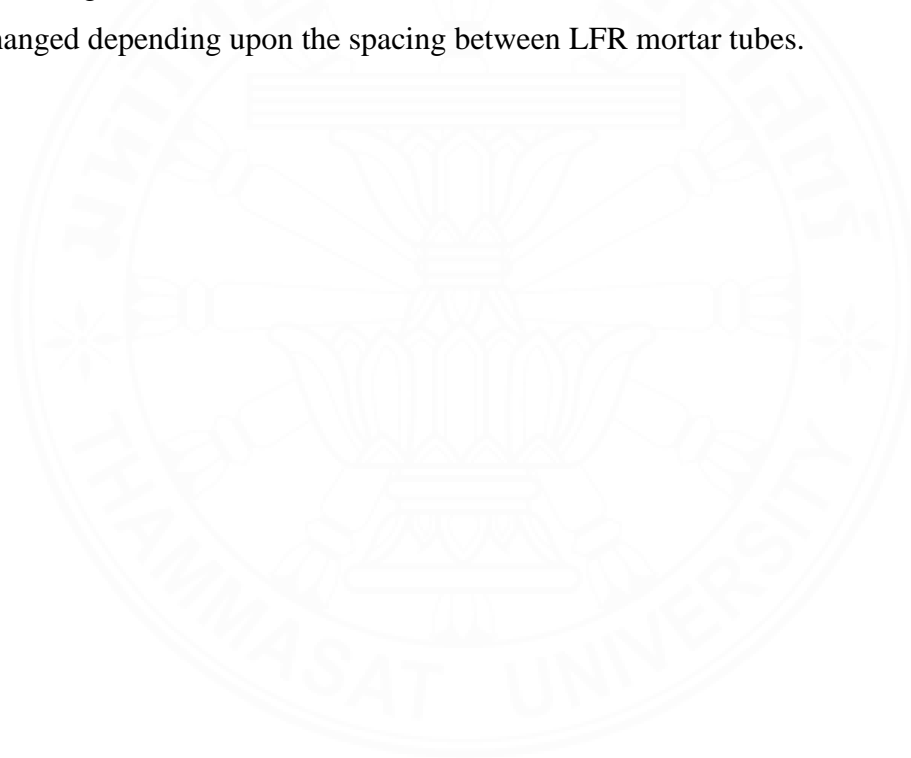


**Figure 2.17** Application of LFR system for road construction [Okamoto, M (2009)]

The applicability of the LFR system was investigated on several occasions. The behavior of the LFR system underneath a railway structure in Japan was studied by Okamoto M. The LFR system was applied to a real scale field carried out on a soft ground of clayey sand. This soil did not meet the requirement of subgrade by Japanese standard (Railway technical research institute 1992) for construction of railway structures. Later, the LFR system was employed in the field to improve the existing soil and then achieve the required satisfactory level. Yoshida T. (2006) investigated the behavior of the LFR system against differential soil settlement. In his study, a load test was performed for the site's soil where the LFR system was applied. His study showed that differential settlement against a locally concentrated vertical load was lowered after the application of the lattice frame system. In another study, Okamoto M. (2016) performed a series of dynamic centrifugal model tests with an LFR system. The results showed that the LFR system was able to minimize differential settlement of the soil subjected to seismic liquefaction. The

system effectively reduced the deformation of the liquefiable soil layer where the improved zone is located under the embankment.

Although Okamoto M. (2009) and Yoshida T. (2006) investigated several applications of the LFR system, the mechanism of the LFR system has not been investigated yet, especially for the long-term effects. Several parameters of the LFR system should be considered in the design of the system, i.e. sizes of the LFR system, the diameter of LFR mortar tube, LFR tube spacing, and effects of injected mortar. The settlement behavior of soil was investigated to identify the effectiveness of the system. The spacing of LFR tubes was a major parameter, according to Okamoto M. (2009) studies. The results showed that soil settlement changed depending upon the spacing between LFR mortar tubes.



## **CHAPTER 3 METHODOLOGY**

This chapter mainly focuses on the collecting methods of field measurements of the experimental embankments, investigation of the material properties of the LFR system, FEM simulations, and comparisons between field and FEA results are the major sections. All the main sections can be summarized as follows,

1. Field measurement data were collected from the two experimental sites located in Samut Sakhon, Thailand. The field data were compared with FEA embankment settlement results. Settlement data of the rock embankment from the field measurements for 30 months were considered in this study.
2. Laboratory tensile tests on LFR underlying sheets and mortar tubes were conducted to obtain their tensile stress-strain relationships.
3. Verification of the finite element model used to simulate soil settlement behavior of embankment without LFR system was performed. A case study from one of the selected references was adopted for this verification. The verified FE modeling method was then used to investigate the settlement of embankment with the LFR system.
4. The FE model of embankment with the LFR system contains different components. Therefore, several material models were used to model the system. Resources such as soil investigation reports and bore log data were used to model different soil layers. Tensile tests of the LFR tubes and LFR sheets were used to construct the material laws for the LFR system.
5. FE model of the LFR system was created based on the assumptions that the LFR mortar tube behaves like a tensile member rather than a flexural member. The stress-strain relationship obtained from the tensile test of LFR tubes was input to the material model of the LFR tube. However, this assumption will later be proved by the analysis results and will be explained in the discussion section.

### 3.1 Experimental program

#### 3.1.1 Embankment test site

Embankment settlement was monitored to investigate the performance of the LFR system and the effects of the LFR mortar tube spacing to reduce embankment settlement. One of the seashore areas of Samut Sakhon province located 50 km from Bangkok, Thailand was selected as the test site (see Figure 3.1).

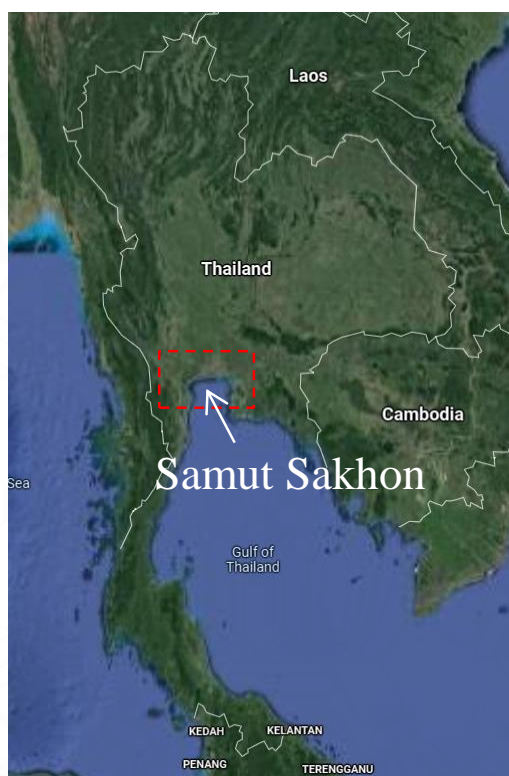


**Figure 3.1** Embankment site (from google maps)

Two rock embankments were constructed on the test site, located approximately 100m apart from each other as shown in Figure 3.2. These two embankments contained LFR systems with different LFR tube spacing arrangements which were  $1\text{m} \times 1\text{m}$  and  $2\text{m} \times 2\text{m}$  (see Figure 3.3). An illustration of the actual LFR system used for the embankment at the test site is shown in Figure 3.4.

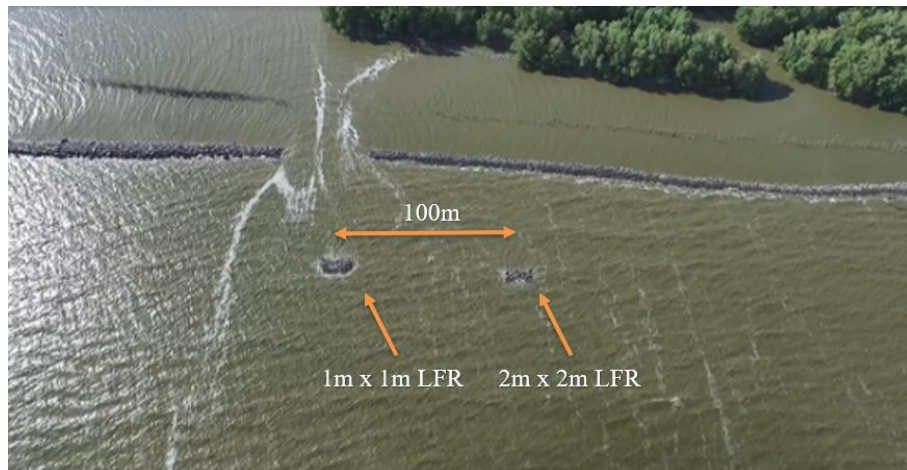


**Figure 3.2** Experimental embankments

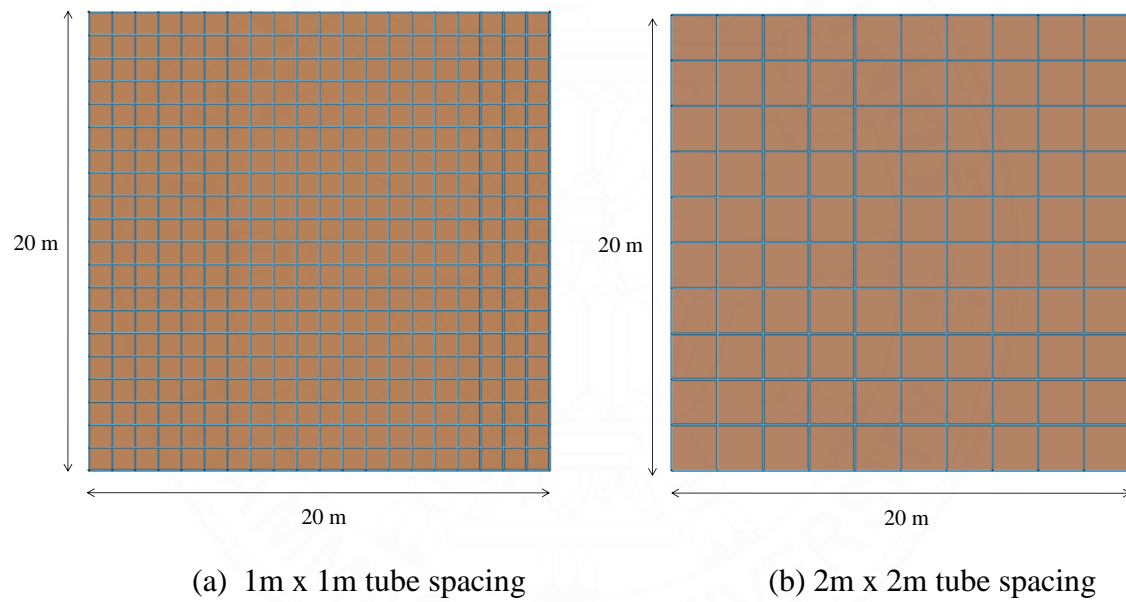


**Figure 3.3** LFR system



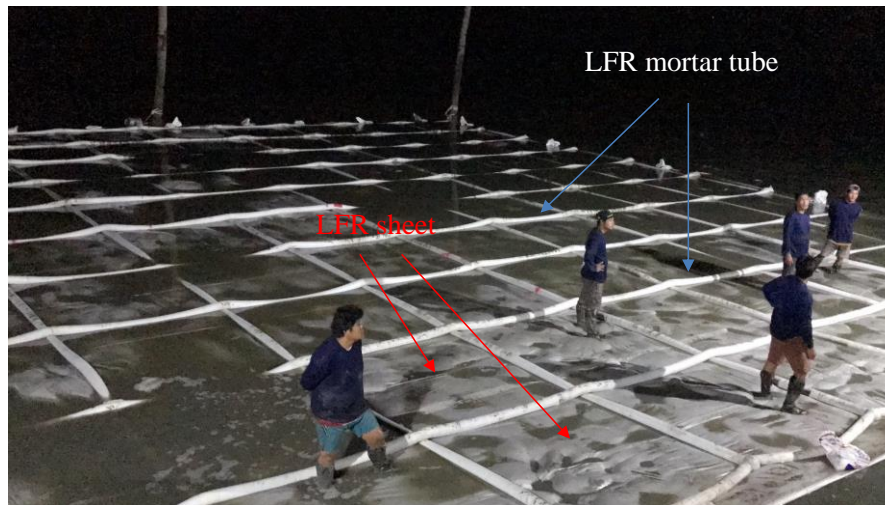


**Figure 3.4** Installation of LFR system at the test site ( $2\text{m} \times 2\text{m}$  tube spacing)

The details of the cross-section of the LFR mortar tube are shown in Figure 3.5. The outside diameter of the LFR mortar tube is 100 mm where the thickness of the LFR tube is 0.7 mm. The thickness of the LFR underlying sheet is also 0.7 mm.

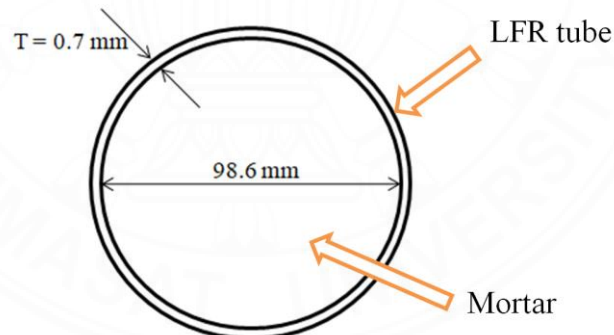


**Figure 3.5** Details of LFR mortar tube cross-section

### 3.1.2 Details of soil investigation

The study location contains two rock embankments with the height of 2m and  $10.5\text{m} \times 10.5\text{m}$  in the plan area. The soil investigation was carried out by STS instruments company limited to determine soil properties of the location and conditions of the site. There are two boreholes, BH-1, and BH-2, where both were 25m in depth. According to the report, there were three different main soil layers

in the soil strata and the site was submerged in water (see Figure 3.6). There are different types of soils existing along the seashores of Thailand. Clay, silty and sandy soils are highlighted among them as mentioned by Surarak, C., (2012).

Several soil samples were collected from the embankment test site for laboratory tests such as consolidation test, unconsolidated undrained tri-axial test, and vane shear test. The examples of soil samples collected for laboratory tests are shown in Figure 3.7. According to laboratory soil tests, several soil types were identified. These soil layers could be categorized as clay, silty clay, and silty fine sand to medium sand. More details of soil investigation are provided in Section 3.3.2.1.

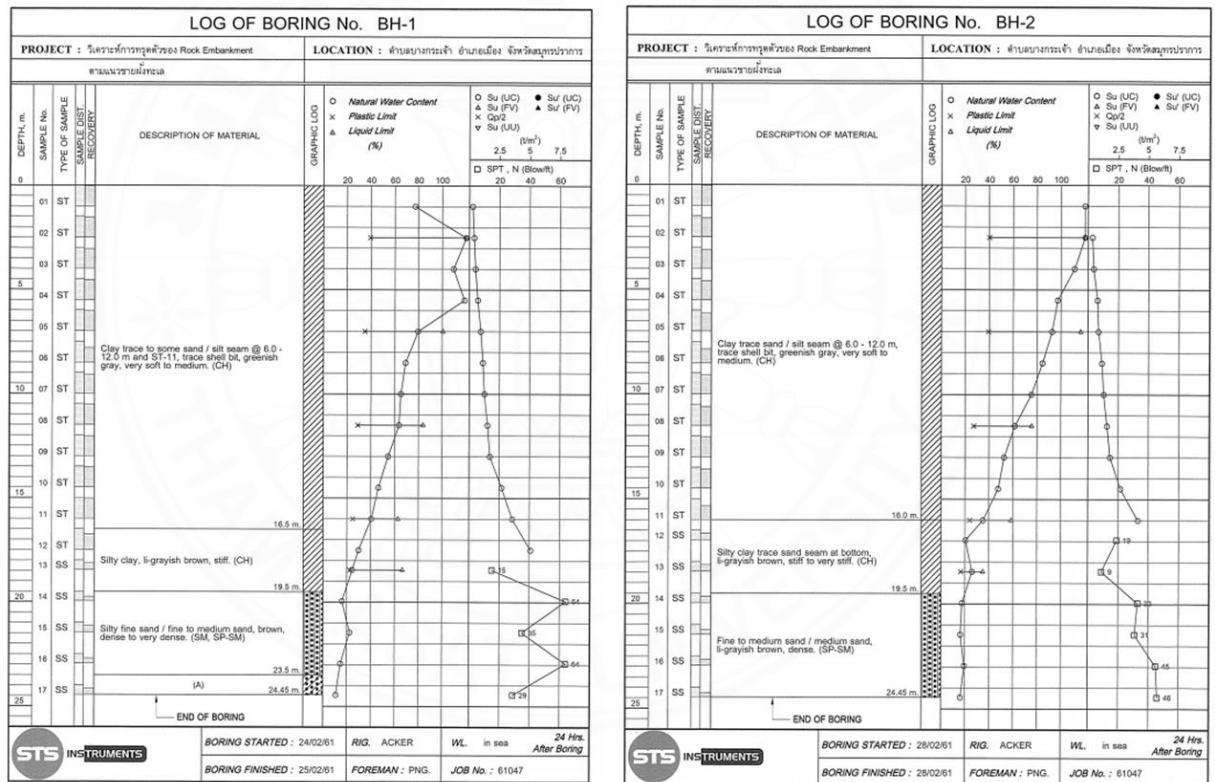


Figure 3.6 Elevation data of bore logs.



**Figure 3.7** Examples of undisturbed soil samples

### **3.1.3 Field monitoring for embankment settlement**

Settlement of the embankments is considered as field measurements for this study. Cumulative soil settlement of two embankments with two different LFR tube arrangements ( $1\text{m} \times 1\text{m}$  and  $2\text{m} \times 2\text{m}$ ) were measured. A brief explanation of the field measurement process was as follows. There were several measurement stations set for this study. Two stations were used to measure the levels of the test embankments (see Figure 3.8). Station 3 was the transfer station from the benchmark reference. TP 3 and TP 4 were used to transfer the level from station 3 to station 4. From station 4, gauge levels of the embankments were recorded. The measurements of gauge levels of embankments were taken at the centers (A1 and B1) and four edges (A2 – A5 and B2 – B5) of the embankments as shown in Figure 3.8. All gauge levels at each embankment were averaged and used to calculate the settlement of each embankment. Gauge level readings of the embankment's settlement were recorded once a week in the first month after the construction was finished. After that, they were taken once a month in the 1<sup>st</sup> year. For the 2<sup>nd</sup> and 3<sup>rd</sup> years, the monitoring was performed once every two months and once every three months, respectively.

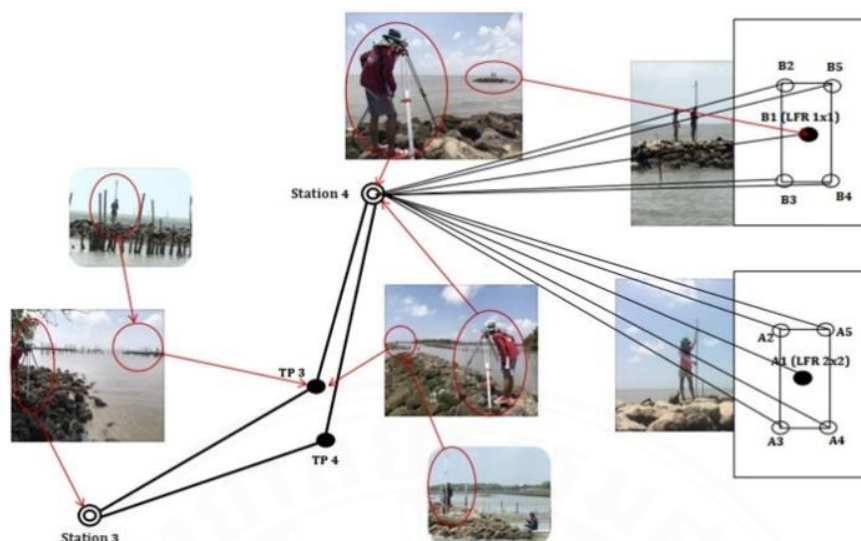


**Figure 3.8** Settlement data collecting procedure.

Currently, the measurement is at the beginning of the 4<sup>th</sup> year after the construction. The measurement is taken twice a year in this phase. The effectiveness of the LFR system was investigated by continuously monitoring and recording the long-term settlement of the embankments for 30 months period.

### 3.1.4 Field measurements of the embankment settlement

Cumulative soil settlement of the two embankments with two different LFR tube arrangements ( $1\text{m} \times 1\text{m}$  and  $2\text{m} \times 2\text{m}$ ) were measured. The test embankments are shown in Figure 3.9. The first measurement was taken 2 days after the construction was completed. Field measurement shows that the embankment with larger LFR mortar tube spacing results in a higher soil settlement (see Figure 3.10).



**Figure 3.9** Embankments with LFR systems being monitored

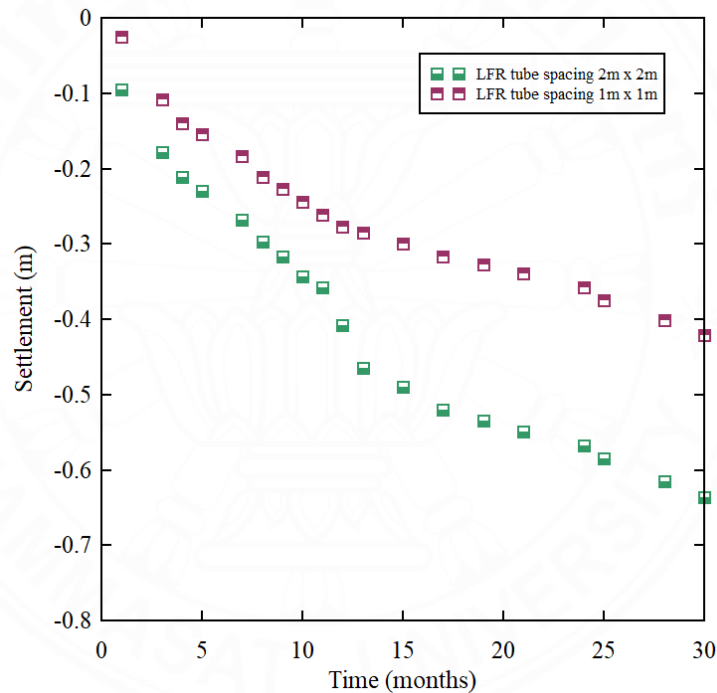


**Figure 3.10** Embankment settlement with LFR systems

### 3.1.5 Investigation of material properties of LFR system by laboratory tests

There are two main components in the LFR system, LFR mortar tubes, and LFR sheets. A tensile test was conducted according to ASTM D3039 for both sample materials, LFR tube and underlying LFR sheet, to determine the stress-strain relationship. Three specimens each were prepared for the LFR tube and the LFR underlying sheet. The speed of tensile grip for tensioning was set to be 2 mm/min

using Universal Testing Machine (Testometric M500-50AT). Tested specimens and test setup are shown in Figure 3.11.

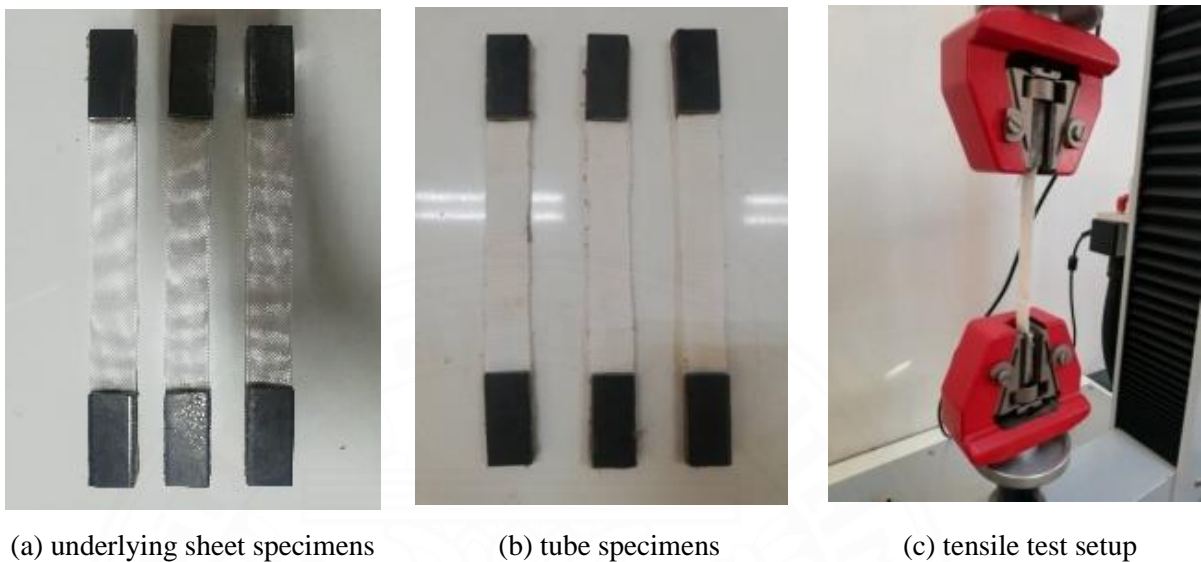


**Figure 3.11** Tensile tests of LFR components.

### 3.1.6 Results of laboratory tests

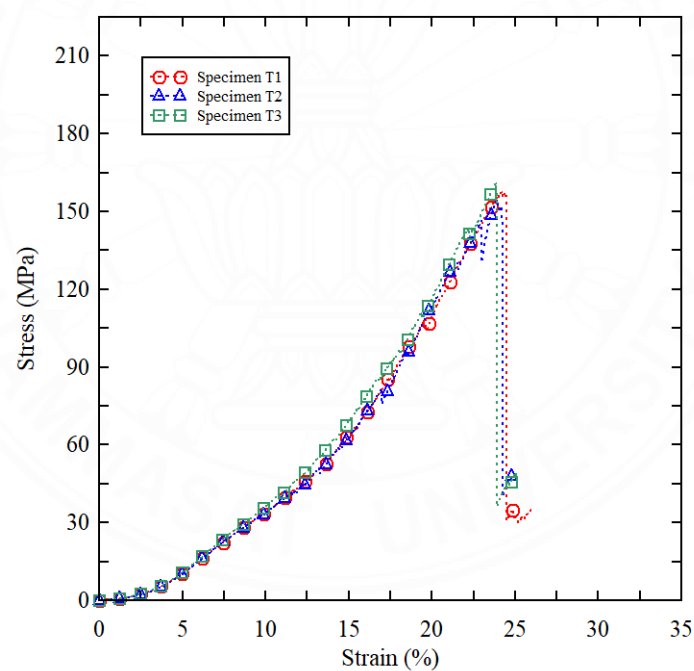
Tensile tests were conducted for two sets of specimens, LFR tube, and LFR underlying sheet specimens. Stress-strain relationship data were collected. Test data show that there are two visible slopes in the stress-strain curves of both the LFR tube and LFR underlying sheet. The stress-strain curve shows a higher second slope in tension after the initial stretching of the LFR tube (Figure 3.12). This second slope continues for a longer period through the total duration of the test and was considered to be Young's modulus of the tested specimen. The failure of the LFR tube specimen is shown in Figure 3.14 (a). The summary of the tested material properties of the LFR tube specimens is shown in Table 3.1. Similarly, the stress-strain curve shows a higher second slope after the initial stretching of the sheet (see Figure 3.13). This second slope continues for a longer period through the total duration of the test. Therefore, the second slope was considered to be Young's modulus of the LFR underlying sheet. The failure of the underlying sheet specimens is shown in Figure 3.14 (b). The summary of material properties of the LFR underlying sheet resulting from the tensile tests is shown in Table 3.2.

**Table 3.1** Material properties of LFR tube

Young's modulus (MPa)	During initial stretch	474.36
	After initial stretch	807.95
Ultimate stress (MPa)	156.9	
Ultimate strain	0.24	

**Table 3.2** Material properties of LFR sheet

Young's modulus (MPa)	During initial stretch	297.32
	After initial stretch	1149.81
Ultimate stress (MPa)	188.28	
Ultimate strain	0.224	

**Figure 3.12** Tensile stress-strain relationship of the LFR tube specimens

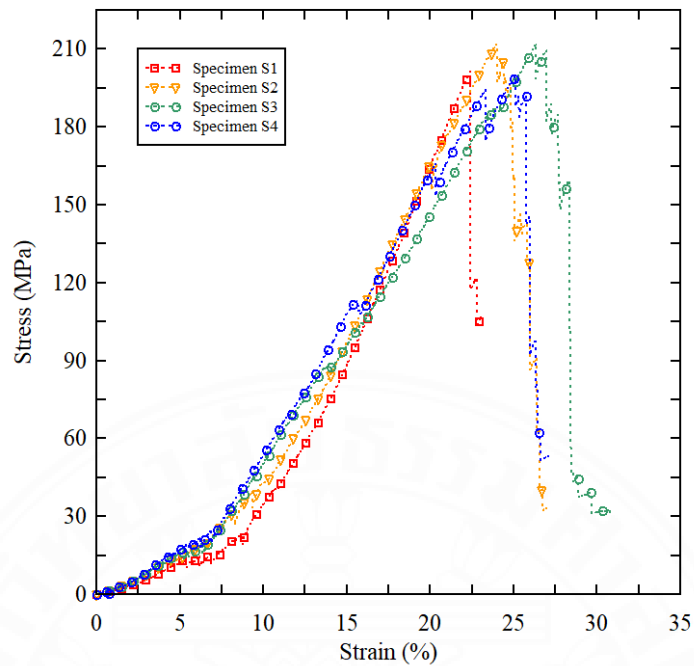


**Figure 3.13** Tensile stress-strain relationship of LFR sheet specimens

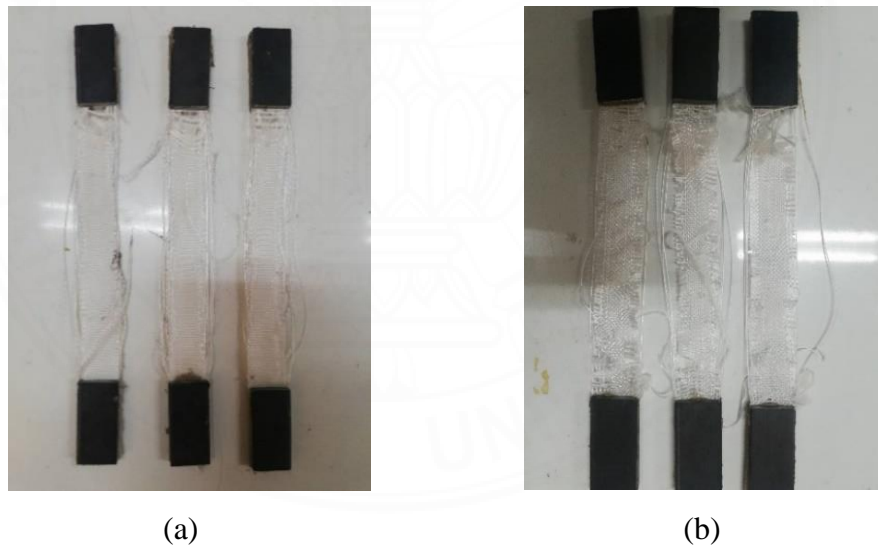


**Figure 3.14** Tested Specimens (a) LFR tubes (b) LFR sheets

### 3.2 Finite element analysis of the verification model

The investigation of the mechanism of the LFR system was the main objective of this study. Therefore, FEM was simulated to study the behavior of the LFR system due to soil settlement under the LFR system. However, before investigating the LFR system, it would be important to correctly simulate long-term



soil settlement of an embankment without the LFR system. Therefore, the verification model was introduced.

A case study originally conducted by Huang W. was selected for this simulation. The LS-DYNA model which contained 3 layers of soil up to a depth of 30m was analyzed. Soil types are mainly sand, and clay contained soils, with different densities and cohesion (see Figure 3.15). Huang, W (2006) conducted a study on the Teven road embankment as adjacently located to the existing pacific highway, 2km from the south of Ballina in northern of New South Wales, Australia. The proposed bypass was located on a flood plain overlying near the mouth of the Richmond River.

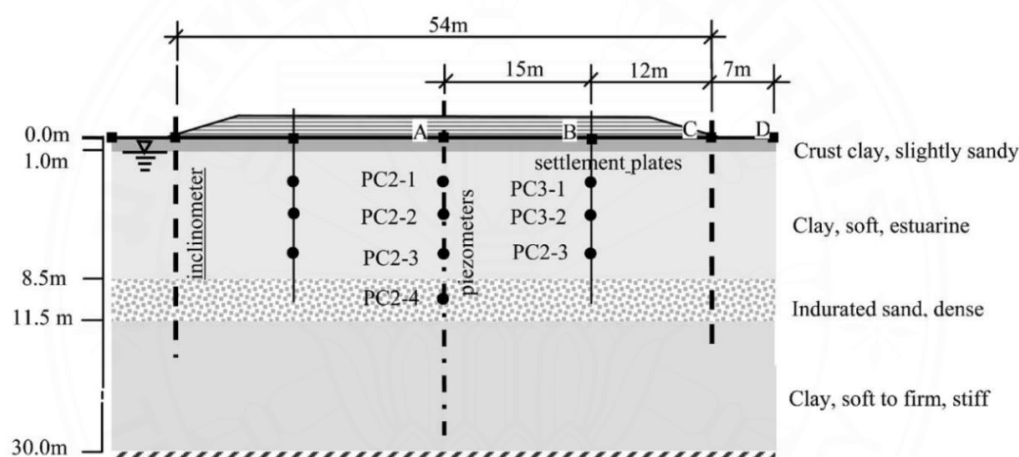


**Figure 3.15** Soil layers and embankment details [Huang, W (2006)]

Time-dependent consolidation soil settlement  $S_c$  takes place under the embankment because of the extrusion of pore water from the void space in soil and reorganization of soil structure. The primary settlement  $S_p$  is the soil deformation observed during the dissipation of excess pore pressure which normally controls a major part of the total consolidation settlement. The secondary settlement  $S_s$  is the continuation of deformation in soil under constant effective stress after the excess pore pressure is tremendously dissipated.

The settlements were monitored for about 1300 days by Huang, W (2006). As the early settlements were well captured by the finite element modeling, it was considered that the total primary consolidation settlement was well predicted by FEM. The Draker-Prager constitute model was employed to simulate soil for finite

element simulations. Several inputs were required for the FE analysis. Those inputs were density, Poisson's ratio, elastic shear modulus, cohesion, and permeability as listed in Table 3.3. The analyzed FE model is shown in Figure 3.16.

**Table 3.3** Material properties of soil and embankment [Huang, W (2006)]

Domain	Depth (m)	E (MPa)	$\nu$	P (kg/m <sup>3</sup> )	$\mu$ (m/s) (e-10)	c (t/m <sup>2</sup> )	G (MPa)
First layer	0-8.5	1.09	0.3	1538	0.165	0.509	0.423
Second layer	8.5-11.5	3.30	0.3	2019	0.001	0.509	1.270
Third layer	11.5-30	49.9	0.3	1630	6.950	0.509	19.20
Embankment	1.6	500	0.3	2500	-	-	24000

Remarks: E is Young's modulus,  $\nu$  is Poisson's ratio,  $\rho$  is density,  $\mu$  is permeability, c is cohesion, G is shear modulus

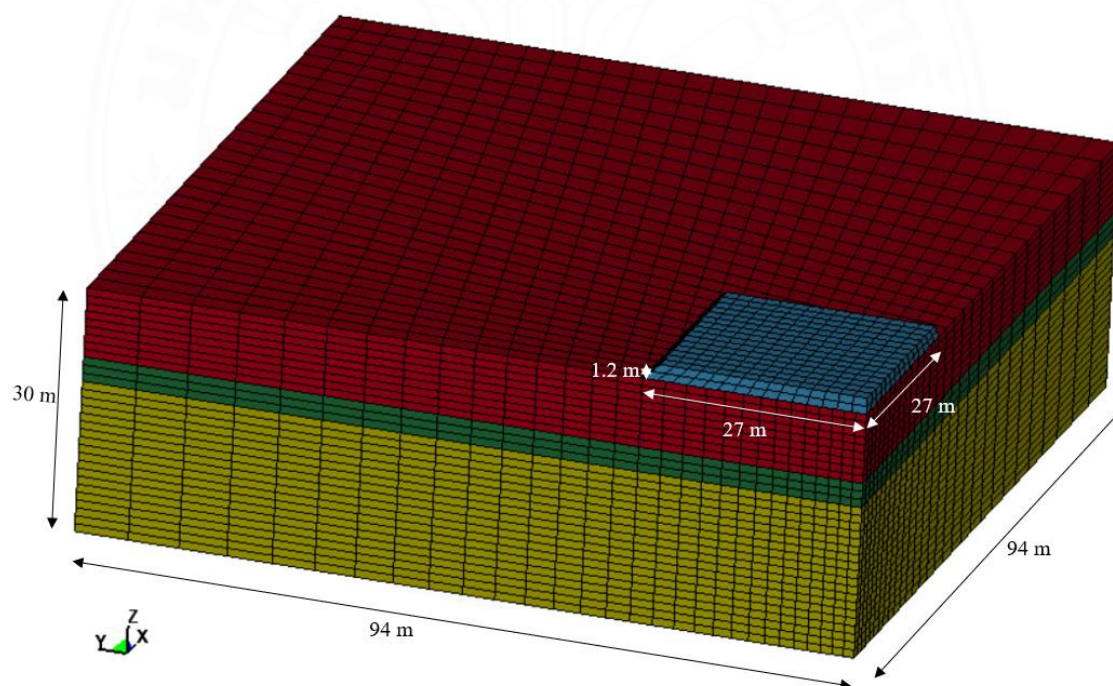


**Figure 3.16** Verification of the FE model without LFR system

A comparison was conducted between the field measurement and the simulated results. The FE simulation results are well-matched with the field measurements as shown in Figure 3.17.

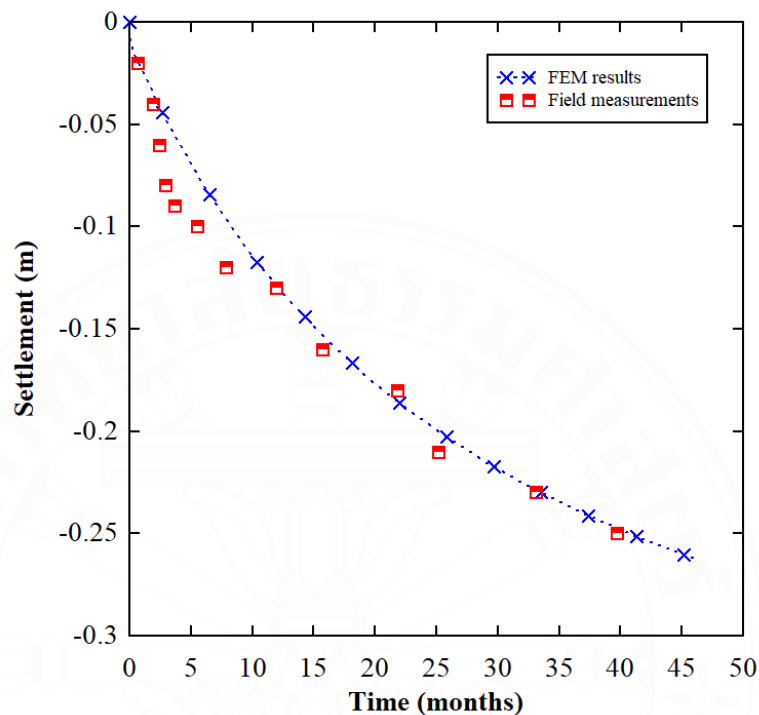


**Figure 3.17** Comparison of FEA results with field measurements

### 3.3 Finite element simulation of the tested embankments with LFR system

The proposed FEM contains several components such as embankment, soil layers, and LFR system. Dimension of the embankment were  $10.5\text{m} \times 10.5\text{m} \times 2\text{m}$ . It had two different slopes to the side of the embankment which were 2:1( $30^\circ$ ) and 1:1( $45^\circ$ ) as shown in Figure 3.18. The LFR system, which includes LFR under laying sheet and LFR mortar tube, was formed as a lattice under the rock embankment. There were two different LFR systems according to the LFR tube spacing. Therefore, two FE simulations were considered.

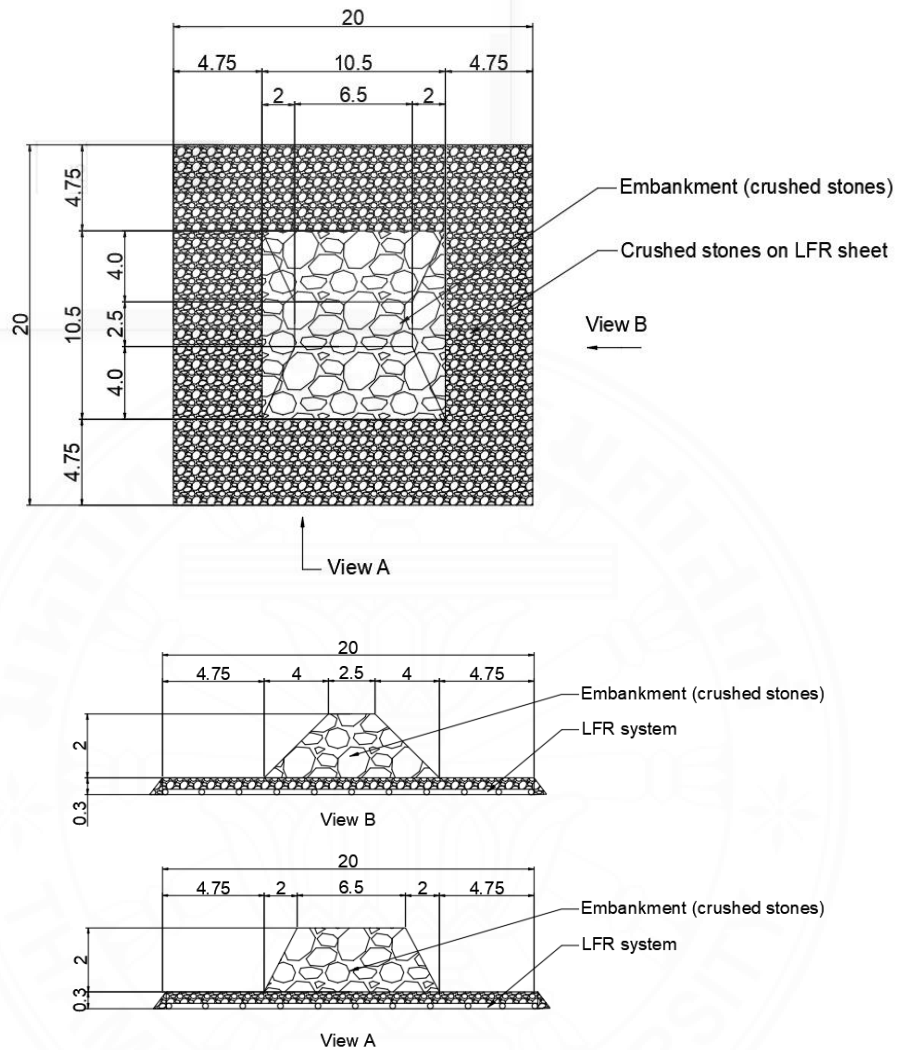


**Figure 3.18** Embankment and LFR system setup (unit in meter)

Another important factor was the contact types. Different types of contacts are used for different interfaces between each component. The interface between LFR underlying sheet and soil surface was considered as a frictional contact whilst a tied contact was used between LFR tubes and sheet. Due to the symmetrical configuration of the model, only a quarter of the full model was simulated.

The soil domains were created according to the soil domains of the verification model following three-dimensional and quarter symmetric soil domains to save computation time. Huang, W. (2006) explained that the soil

domain should be larger than three times the width of the embankment so that the boundaries have negligible influence on the results. Therefore, all FE models followed this concept. The model contained three main FE components which are three different soil layers, embankment, and LFR system as shown in Figure 3.19.

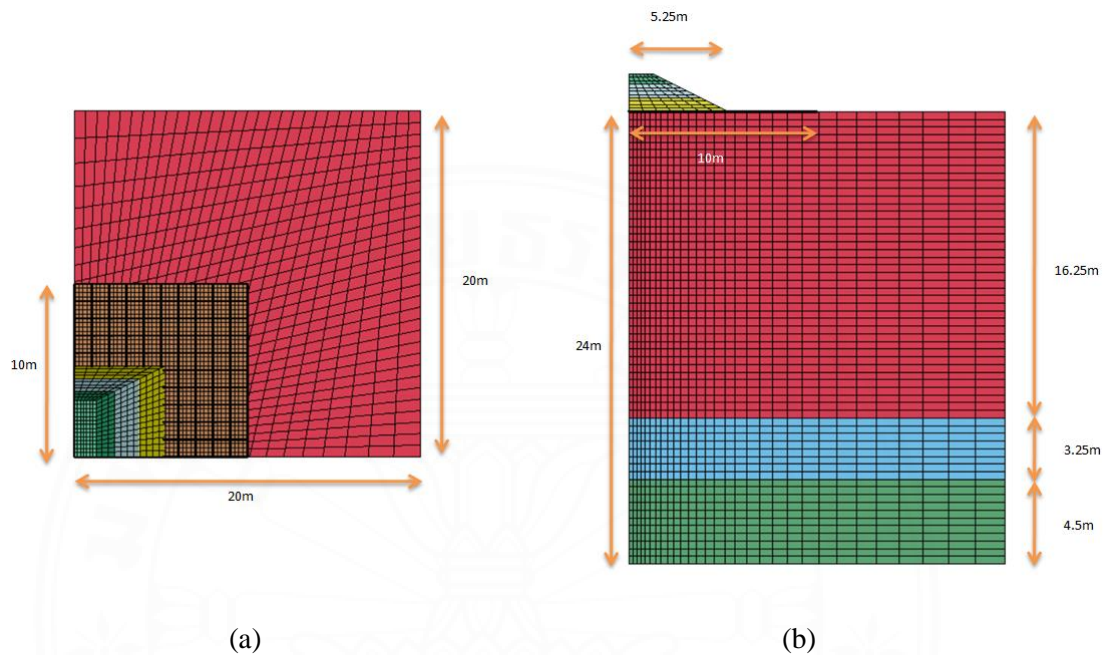


**Figure 3.19** Studied finite element model (a) top view (b) side view.

FEA can be conducted considering a model of composite LFR mortar tube. If there is no separation or slip between the mortar and the tube, a perfect bond between these two components can be considered in the FE model. Initially, after injection of mortar into LFR tubes, a considerable amount of liquid mortar infiltrates into the tube fabric. Once the infiltrated mortar is hardened, it initiates a perfect bond between the mortar and the tube. However, the perfect bond condition is not valid when the mortar cracks because relative displacement between the mortar surface and the inner surface of the tube can occur in the vicinity of the cracks, indicating inappropriacy for assuming perfect bond contact condition. When mortar cracks, the contact type assigned to the model starts to disagree with the constitutive law. Therefore, it is not possible to follow the same constitutive law throughout the total simulation period. Contact between cracked mortar and the tied tube is a complex contact to simulate. For this reason, a simple LFR mortar

tube concept is required for FE analysis. As a solution for this issue, the tension stiffening concept was introduced to simulate the stress-strain relationship of LFR mortar tubes. Therefore, the LFR mortar tube is simulated by only considering the LFR tube with tension stiffening effects contributed from the cracked mortar.

Generally, a tension stiffening behavior can be observed in reinforced concrete (RC) members where it can be defined as the increase in apparent stiffness of steel in an RC member due to the stress transfer between reinforcement and concrete through bonding between cracks of these two components. Figure 3.20 shows typical examples of apparent steel stiffness enhancement resulting from tension stiffening in RC members. The level of increase in the stiffness depends on the bonding condition between concrete and reinforcement (generally concrete strength) as well as reinforcement ratio (Massicotte et al., 1990). Tension stiffening behavior is often implemented for cracked RC structures. The stresses in a bar embedded in concrete are usually non-uniform after concrete cracks. High steel stresses are found in the crack locations while they are lower in between cracks, so the concept of average stress vs average strain of steel is applied by considering tension stiffening effects from the concrete in between cracks.

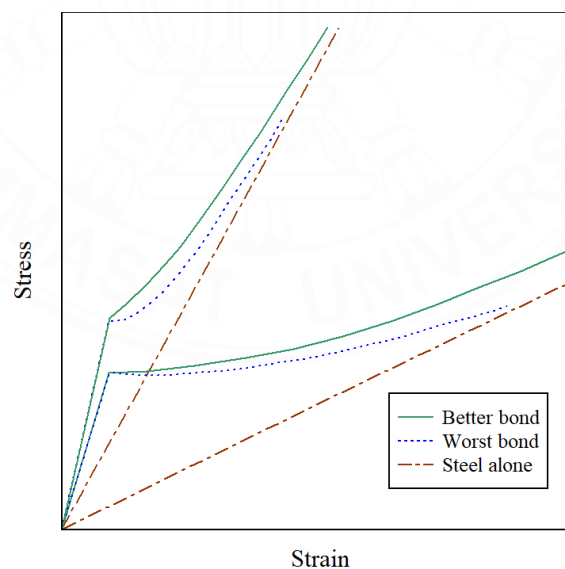


**Figure 3.20** Tension stiffening effects in RC members [Massicotte et al., 1990]

It is assumed here that LFR tubes with cracked mortar in the LFR system behave similarly to the reinforcement in the cracked RC members in enhancing the

stiffness of the LFR mortar tube after the mortar has cracked. This behavior replicates tension stiffening behavior in cracked reinforced concrete. However, there is still no existing model for the LFR tubes to express the bond distribution between cracks and to explicitly define the average stress vs average strain relationship. Therefore, several repetitive calculations are required to generate a suitable average stress-strain relationship of LFR tube with tension stiffening effects for the FEA in this study.

### 3.3.1 Element types, sizes, boundary conditions, and contacts of FEM

In the FE model, the soil domain has meshed where the mesh density was increased from underneath the center of the embankment outward to all boundaries. The range of element sizes was considered for each FE component. Element sizes of LFR tubes and the mortar were smaller than those of other components. Summary of the element sizes for all components are listed in Table 3.4. It was important to keep similar element sizes in the contact regions of different components to minimize the possible numerical instabilities and maximize the simulation accuracy.

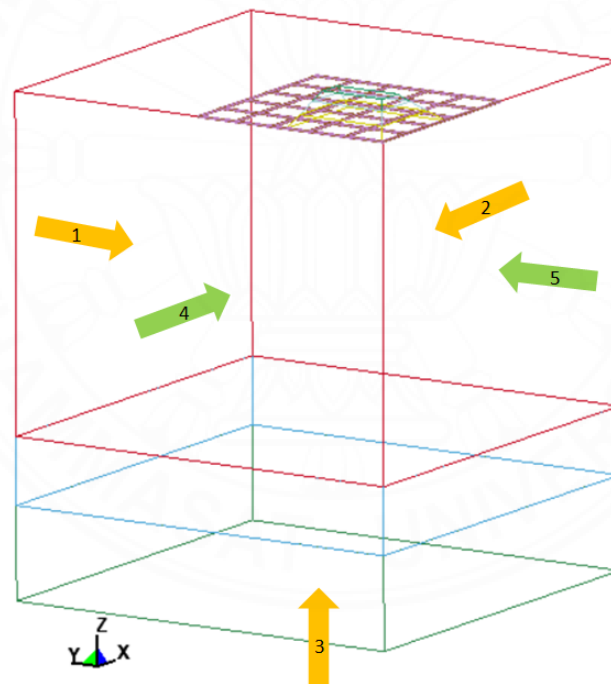
**Table 3.4** Average element sizes

Component	Element size (m)
Soil domain	0.19 – 1.56
LFR sheet	0.25
LFR tube	0.16
Mortar	0.16
Embankment	0.17 – 0.69

Several boundary conditions were applied to the developed finite element model. Firstly, boundaries at the x- and y-sides and the base plane of the soil domain were constrained in all directions (see Figure 3.21) as used by Okamoto M. et al. (2016). The nodes on the planes indicated by arrows 1, 2, and 3 were constrained in X-, Y-, and Z directions. The symmetric planes of the FE model were the planes demonstrated by arrows 4 and 5. These planes were restrained in

translation in the directions of X- and Y- directions, respectively. The width of the soil domain should be minimum of three times the embankment width so that the boundaries at the edge sides will have a negligible influence on the simulation results Jiang, H., & Zhao, J. (2015). Self-weight of the embankment acts as applied pressure to the underneath soil.

Contacts between components were crucial for a realistic simulation. Different contact types were used in the FE model of the embankment with the LFR system. The contact between LFR underlying sheet and underneath soil was considered as a frictional contact. The contact between LFR underlying sheet and the LFR mortar tube was tied since the sheet and tube were knitted together and no detachment/slip between these two components was allowed. Body domains and contact types assigned are shown in Figure 3.22 and listed in Table 3.5.

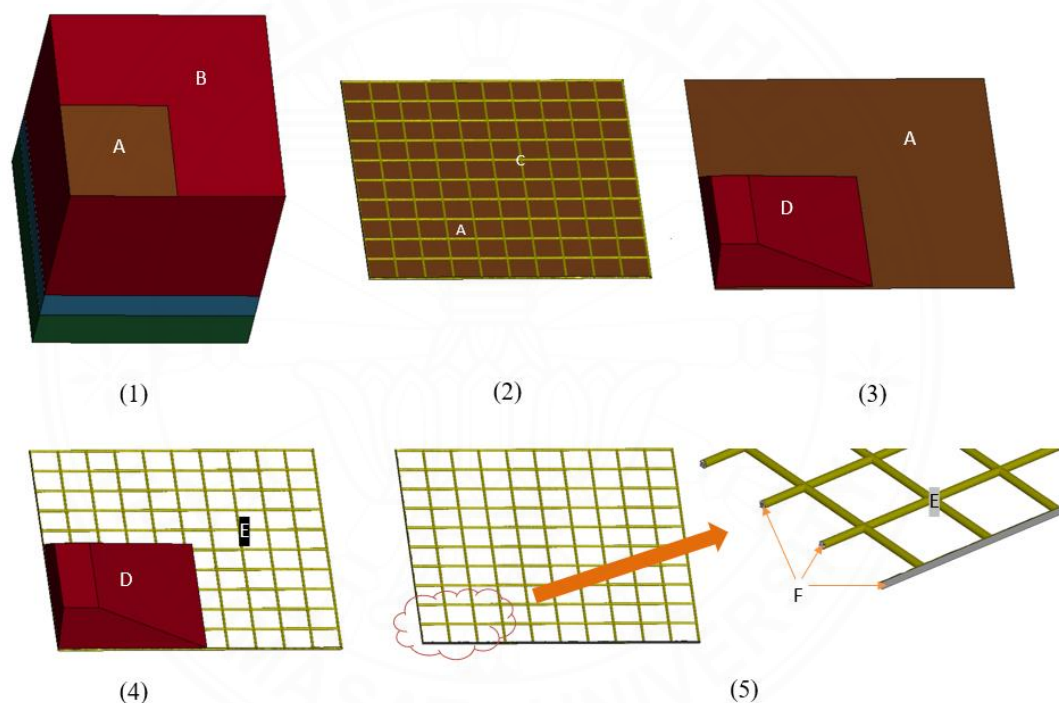


**Figure. 3.21** Demonstration of boundary conditions of the FEM



**Table 3.5** – Contacts and types of FEM

No.	The interface between each FE component	Type of contact
1	LFR underlying sheet – soil surface	Frictional contact
2	LFR underlying sheet – LFR mortar tube	Tied contact
3	LFR underlying sheet - Embankment	Bond contact
4	LFR tube - Embankment	Bond contact
5	LFR tube - mortar	Bond contact

**Figure 3.22.** Contact types used in the FE model in this study (refers to Table 3.5)

### 3.3.2 Material models

There are several components in the LFR system such as LFR tubes, LFR underlying sheet, and mortar. Therefore, different material models were required to conduct finite element simulations. Selected material models and properties gathered for these components are discussed in this section.

### 3.3.2.1 Soil layers and embankment

Based on soil testing, there are three soil layers considered for the FEM. The first soil layer (clay) was the thickest soil layer having 16.25 m in thickness and the most influential layer to produce settlement because embankment self-weight directly acts on it. The other two soil layers (silty clay and silty fine sand) were relatively thin having thicknesses of 3.25 m and 4.5 m, respectively. The Drucker-Prager (DP) constitutive model was employed to simulate the soil layers. The material parameters of the DP model are listed in Table 3.6. These material properties were obtained from the soil boring log of the site. The embankment was 2 m in height and modelled with elastic material properties. The embankment was constructed from rock and boulders having a bulk density of 2200kg/m<sup>3</sup>. An embankment was modelled as an elastic component in the FEM.

Many LS-DYNA's capabilities for civil engineering analysis have been developed in recent years. These developments include material models for reinforced concrete and soils. Several soil analysis types are available in LS-DYNA such as undrained, drained, and time dependent consolidation analysis. Among the available types of analysis, the time dependent consolidation analysis was applied to this study. Material characteristics of soil such as those containing pore fluids and pore pressure were important soil characteristics required for long term settlement simulation. Another important parameter considered for soil simulation was the permeability of the soil layers. This parameter was crucial to simulate long term settlement behavior of soil. Therefore, three sets of data for three soil layers listed in Table 3.6 are contemplated in the analysis.

**Table 3.6** Soil and embankment properties of FEM

	Depth (m)	E (MPa)	$\nu$	P (kg/m <sup>3</sup> )	$\mu$ (m/s) (e-10)	c (t/m <sup>2</sup> )	G (MPa)
First layer	0-16.25	1.73	0.3	1495	7.461	2.08	0.276
Second layer	16.25-19.5	6.22	0.3	1766	0.897	5.73	2.39
Third layer	19.5-24	9.00	0.3	1881	0.897	5.73*	3.46
Embankment	2	500	0.3	2200	-	-	24000

Remarks: E is Young's modulus,  $\nu$  is Poisson's ratio,  $\rho$  is density,  $\mu$  is permeability, c is cohesion, G is shear modulus

Input soil parameters were obtained from laboratory test results. Young's modulus ( $E$ ) of each soil layer was calculated using SPT N-values from the borehole chart. The samples were tested under drained condition. The density ( $\rho$ ) of each soil layer was obtained from the laboratory test results. The permeability ( $\mu$ ) of each soil layer was calculated from the consolidation test report. The cohesion ( $c$ ) of soil was obtained from unconsolidated undrained (UU) triaxial compression tests. Shear modulus ( $G$ ) was calculated from Young's modulus and Poisson's ratio.

### 3.3.2.2 LFR underlying sheet

The domain of the LFR underlying sheet is shown in Figure 3.23. An average stress-strain relationship of the LFR sheet obtained from the tensile tests as shown in Figure 3.24 was used as the input of MAT 24 or MAT PIECEWISE LINEAR PLASTICITY to model the LFR sheet. The LFR sheet's material properties for FEM input are shown in Table 3.7.

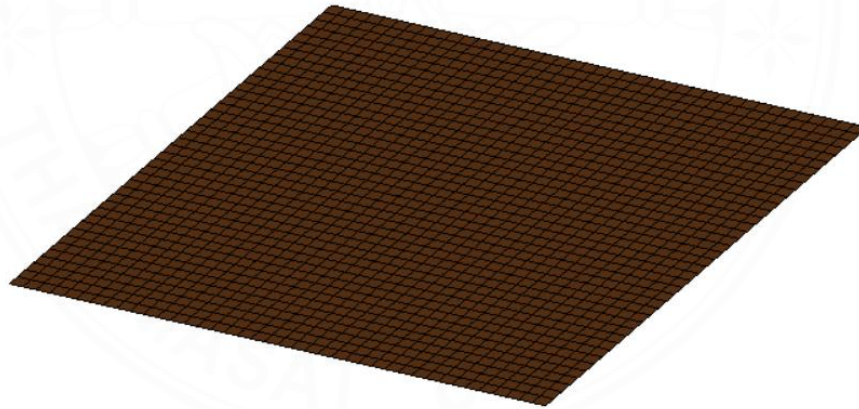


**Figure 3.23** LFR underlying sheet

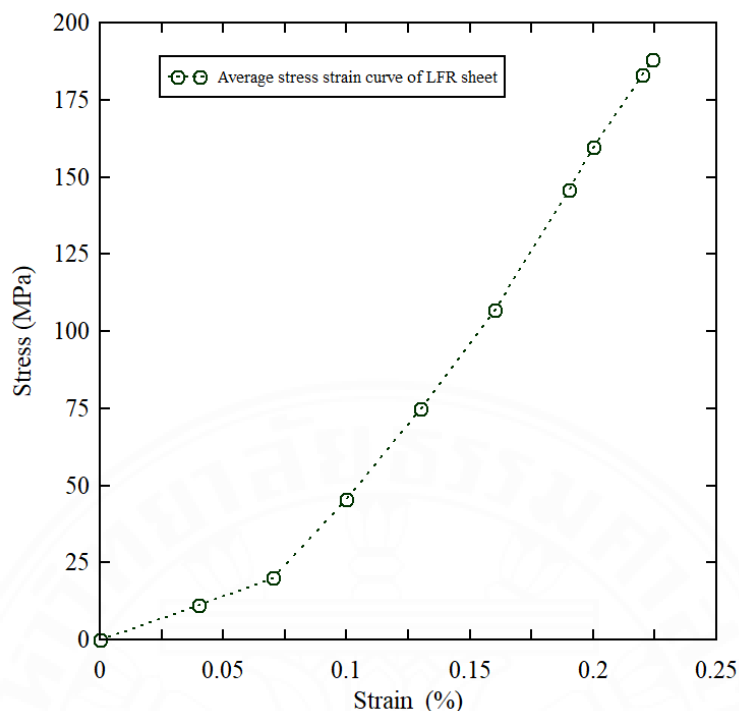


**Figure 3.24** Stress-strain curve of LFR sheet

**Table 3.7** General information of LFR sheet

Component name	Element type	Density (kg/m <sup>3</sup> )	Poisson's ratio	Strength (MPa)
LFR sheet	SHELL	620	0.4	188

### 3.3.2.3 LFR mortar tub

LFR mortar tube contains both LFR tube and mortar as shown in Figure 3.25. This study investigates two approaches used to model the LFR mortar tube which were indicated as FE analysis case 1 and case 2 in the next section. The LFR tube was modelled with MAT 24 - MAT PIECEWISE LINEAR PLASTICITY in both analysis cases. MAT 159 - MAT CSCM was used to model the mortar inside the LFR tube in analysis case 1. However, there was no mortar component explicitly modelled in analysis case 2 since the contribution of the mortar was considered through the modified (average) stress-strain curve of the LFR tube with tension stiffening effects. The material parameters for the LFR mortar tube will be provided in the next section.

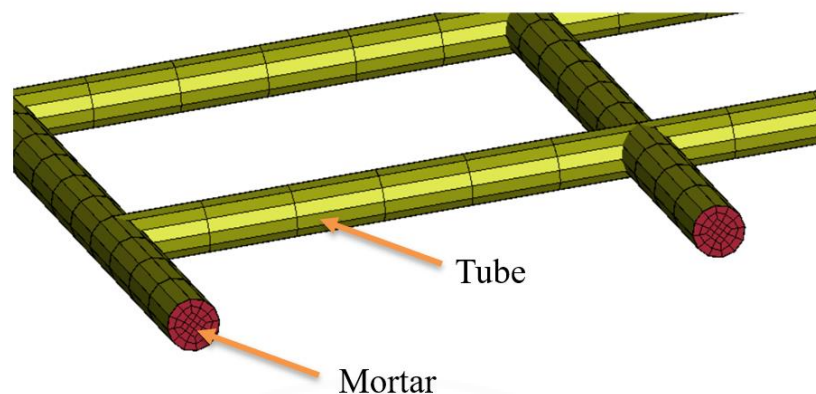


**Figure 3.25** LFR mortar tube composite

### 3.4 Finite element analysis cases

The analysis of FEM was conducted in two cases. These two cases were considered for different concepts of LFR mortar tube modeling while other components (LFR sheet, rock embankment, soil layers) were identically modeled in these two analysis cases. Case 1 considers the composite LFR mortar tube by modelling mortar and LFR tube in separate domains. Case 2 considers only the LFR tube without mortar but with tension stiffening effects included in the constitutive law of the LFR tube.

#### 3.4.1 Case 1 – Simulation of LFR mortar tube by modeling both LFR tube and mortar

LFR tubes and mortar were modeled as two separate domains as shown in Figure 3.25. MAT 24 model was assigned to the LFR tube considering the average stress-strain relationship of the LFR tube obtained from the tensile tests as shown in Figure 3.26. The mortar domain was simulated using MAT 159 model where the damage patterns in mortar can be observed through resulted effective plastic strain. The summary of material properties of both LFR tube and mortar domains is shown in Table 3.8. The tied contact was assigned along with the interface between mortar and tube domains by assuming a perfect tied bond. With this modelling approach, the effects of the quality/grade of concrete on the performance of the LFR system can be investigated.

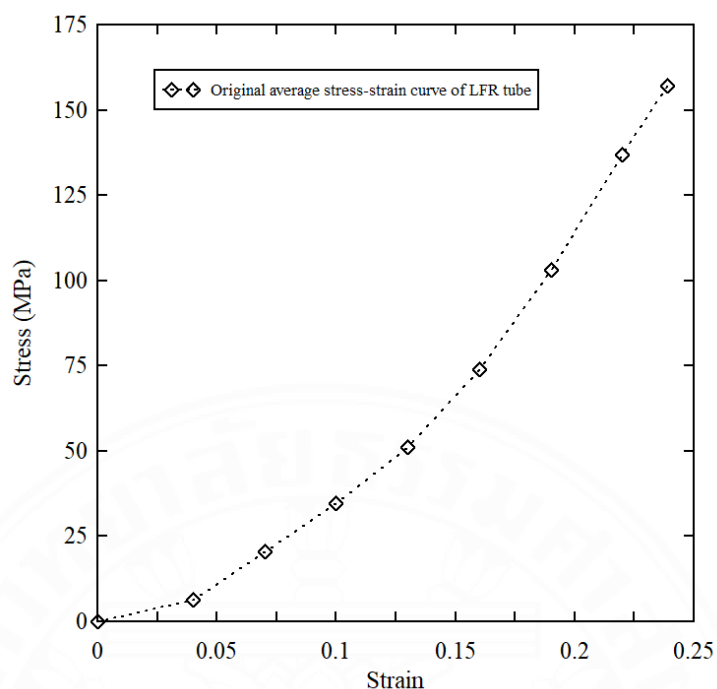


**Figure 3.26** Stress-strain curve of LFR tube

**Table 3.8** – Summary of material properties for LFR mortar tube in analysis case 1

Component	Density (kg/m <sup>3</sup> )	Poisson's ratio	Strength (MPa)
LFR tube	1,046	0.4	Tensile strength = 155
Mortar	2,250	0.2	Compressive strength = 30

However, since the LFR mortar tube consists of injected mortar in the LFR tube, actual contact between mortar and tube was complicated to assign in numerical modeling since the contact behavior was not expected to remain the same throughout the simulation period. Even though the most realistic modeling approach was to model LFR tubes and mortar explicitly, the model should be able to trace local slip between mortar and LFR tubes caused by mortar cracking, which was very complicated. Once slip takes place, a contact that considers the real behavior of interface stress and interface slip should be activated in that model region. In addition, this method requires a significant large number of elements to

model for both LFR tubes and mortar. Therefore, as a solution, analysis case 2 is introduced with the consideration of tension stiffening effects.

### 3.4.2 Case 2 – Simulation of LFR mortar tube by modeling of LFR tube with tension stiffening effects

LFR mortar tube without mortar domain was considered in analysis case 2. The diameter of the LFR tube considered in the model was 100 mm which was the same as that of the actual tube. Figure 3.27 shows the LFR tube domain used in analysis case 2. Since case 2 only considers LFR tube (without mortar), there should be a modification for the stress strain relationship to enhance the tube stiffness by the effect of cracked mortar.

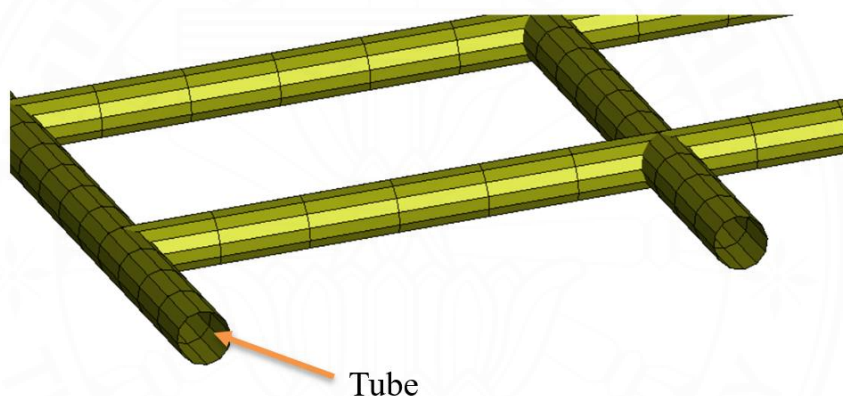


**Figure 3.27** LFR tube in analysis case 2

During the injection of the mortar into the LFR tube, a certain portion of liquid mortar was absorbed by the tube fabric and hardened, initiating a bond contact between the mortar and the LFR tube. The mortar contributes to the enhancement of stiffness of the composite LFR tube. Since mortar is very weak in tension, the tensile strength of this composite system mainly relies on the tensile strength of the polyester tube while the tensile capacity of the mortar can be integrated into the tensile stress-strain relation by the concept of tension stiffening. Therefore, the stiffness of the cracked mortar tube must be implemented. This stiffness was slightly higher than the stiffness of the bare tube. The stiffness enhancement of the LFR tube by the mortar was not constant throughout the entire stress-strain relationship but depended on the level of severity of cracking. The

stiffness of the LFR tube is enhanced significantly by the mortar during the initial stage of service (low stress level in the LFR tube) when the mortar is still uncracked. After mortar cracks, however, enhancement in stiffness of the system becomes less and finally, stiffness approaches the level of standalone LFR tube when the cracking was very severe at high tensile strain. It is noted that in addition to the cracking of mortar, slippage along with the mortar and LFR tube interface at the vicinity of cracks also degrades the level of stiffness enhancement of this composite system. This behavior is similar to tension stiffening behavior observed in RC members. Therefore, modelling of LFR mortar tube can be performed with the concept of stiffness enhancement due to tension stiffening effects in a similar manner to modelling concept of RC members.

The proposed tension stiffening (TS) stress-strain curve used to simulate the behavior of LFR mortar tubes was modified from the original stress-strain curve of the LFR tube obtained from the tensile tests. Figure 3.28 shows the proposed TS curve compared to the original stress-strain curve of the tube.

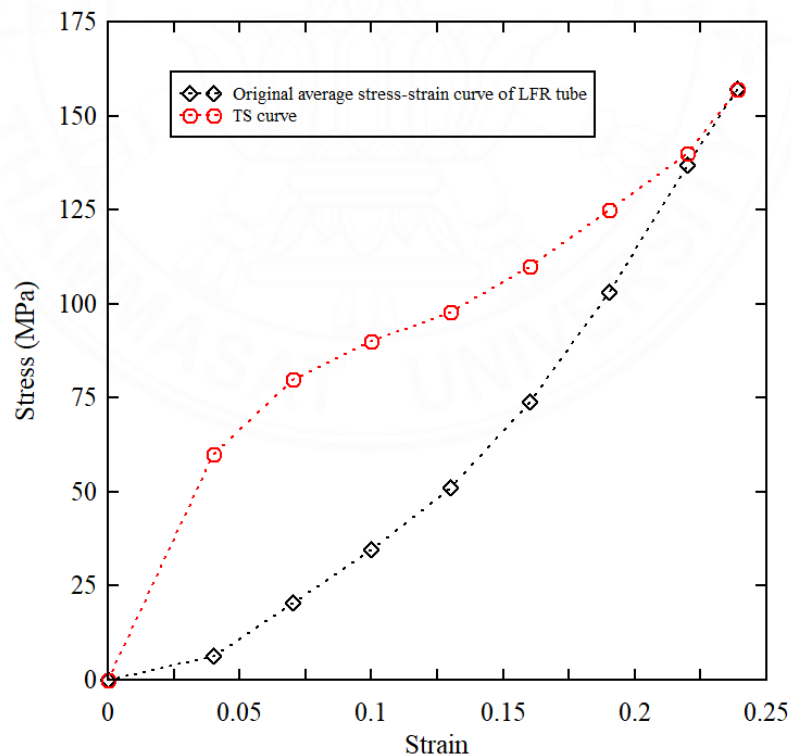


**Figure 3.28** Proposed tension stiffening (TS) stress-strain curve to model the LFR tube by incorporating the contribution of cracked mortar



The stiffness of the TS curve is enhanced significantly to be much higher than that of the original curve of the bare tube during low levels of stress and strain which corresponds to the state of uncracked mortar. In other words, stiffness enhancement is due to the contribution of uncracked mortar bonded to the tube which is not modelled explicitly in the FE model. However, once the mortar cracks at a higher strain level, the contribution of cracked mortar to enhance the stiffness of the LFR tube gradually decreases. Finally, the stiffness of the LFR mortar tube is the same as that of the original LFR tube at the ultimate condition as shown in Figure 3.28. It is expected that the proposed TS stress-strain curve of the LFR tube will avoid underestimation of soil settlement from analysis case 1 which assumes perfect bonding between the LFR tube and mortar during this long-term settlement as the mortar can crack at some states after loading of the rock for embankment construction. In addition, the FE model in analysis case 2 contains smaller number of elements since there is no mortar in the FE model. Therefore, it is more efficient in terms of computational resources used to analyze this model compared to that of analysis case 1. Both original stress-strain curve and enhanced stress-strain curve considering tension stiffening (TS) were used to represent LFR mortar tubes. The FEMs with these two modelling approaches were introduced as Case 2– original curve, and Case 2 – with modified TS curve. Material card - MAT 24 was employed to input these curves into the models.

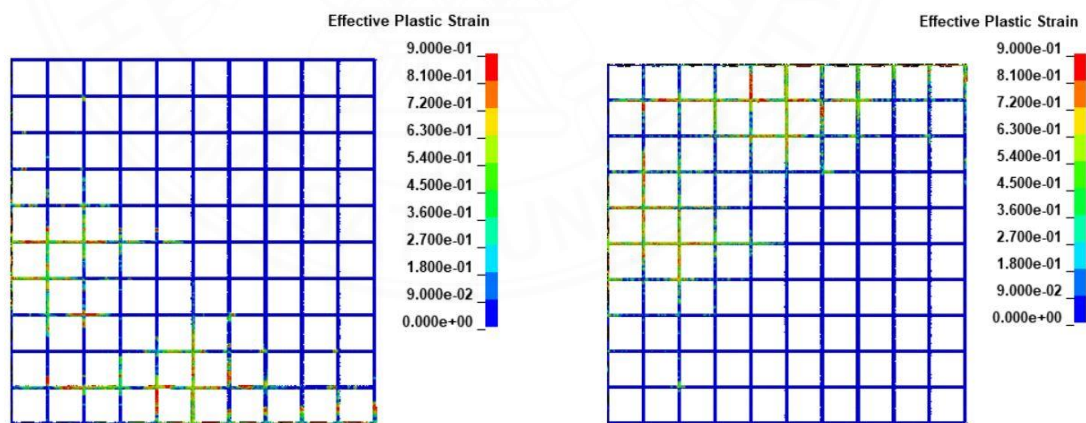
## CHAPTER 4

### RESULTS AND DISCUSSION

#### 4.1 Investigation of mortar damage

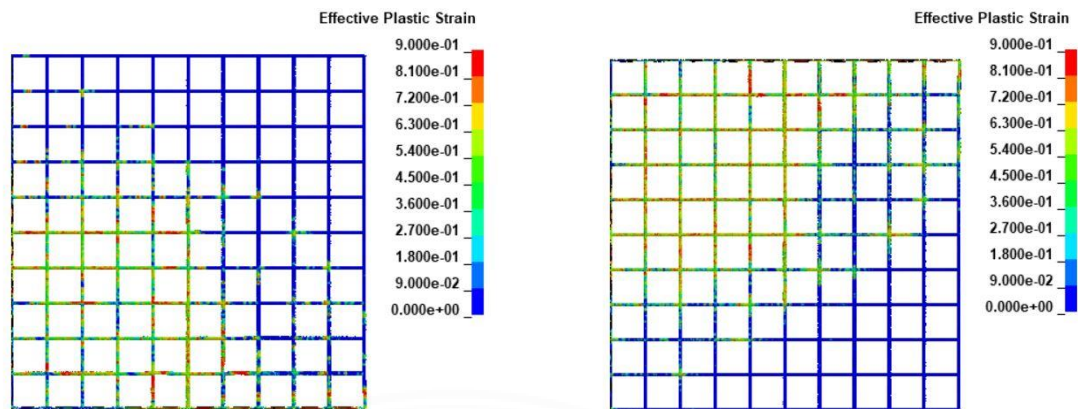
The main purpose of the FEM simulation was to understand the mechanism of the LFR system. Because once the LFR system was installed under the embankment, it was difficult to monitor and inspect the condition of the LFR system after construction. Therefore, the FEM simulation helped to understand the mechanism of the system. Moreover, it can verify the damage of mortar in the LFR system. The damage of mortar can be demonstrated in terms of effective plastic strain. The effective plastic strains of mortar viewed at the top and bottom at 4 days and 7 days after completion of embankment construction are shown in Figure 4.1.

As shown in Figure 4.1, the effective plastic strains increase dramatically from 4 days to 7 days, and the damage is expected to continue. To be exact, effective plastic strains in Figure 4.1 show the damage of mortar in tension as the LFR members subjected to tension in this setup. In addition, the FE results also indicate tensile stresses in both LFR tubes and LFR sheets which confirm that both components are tension members.



(a) Top view of mortar after 4 days

(b) Bottom view of mortar after 4 days



(c) Top view of mortar after 7 days

(d) Bottom view of mortar after 7 days

**Figure 4.1** Damages of mortar in terms of effective plastic strain

Furthermore, from the FE results, it can be stated that, in the first 4 days, mortar is 30% damaged and it increased to more than 50% by the period of 7 days. Therefore, if mortar was damaged in the LFR system in a short period, then the mortar cannot resist bending but can only support the LFR tubes to resist the embankment settlement in tension via the tension stiffening mechanism.

#### 4.2 Stress investigation of LFR system

It is important to investigate the stresses in the LFR system to understand the behavior of the LFR tubes and LFR sheet. Locations where the mortar was highly damaged (see Figure 4.2), were selected and relevant locations in the LFR tube were investigated. Therefore, stresses in the LFR tube were observed. Stresses at both top and bottom of the tube were plotted as shown in Figure 4.3. The stress components in both X- and Y- directions at the top and bottom of the tube were both positive which indicates tensile stress at both top and bottom of the tube. Therefore, the LFR tubes in the LFR system was confirmed to work mainly as a tensile member.

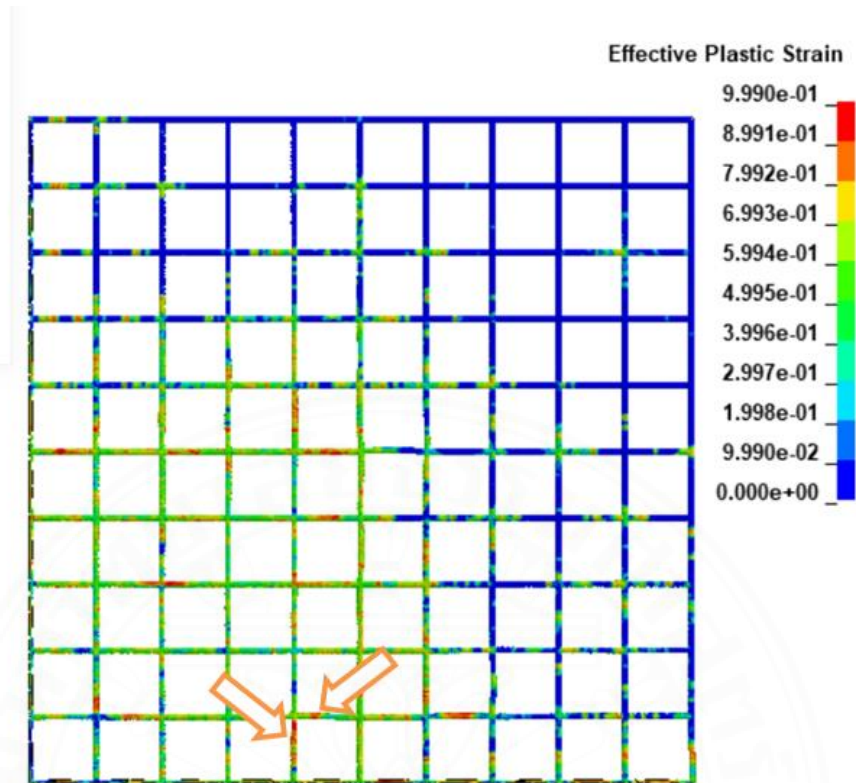
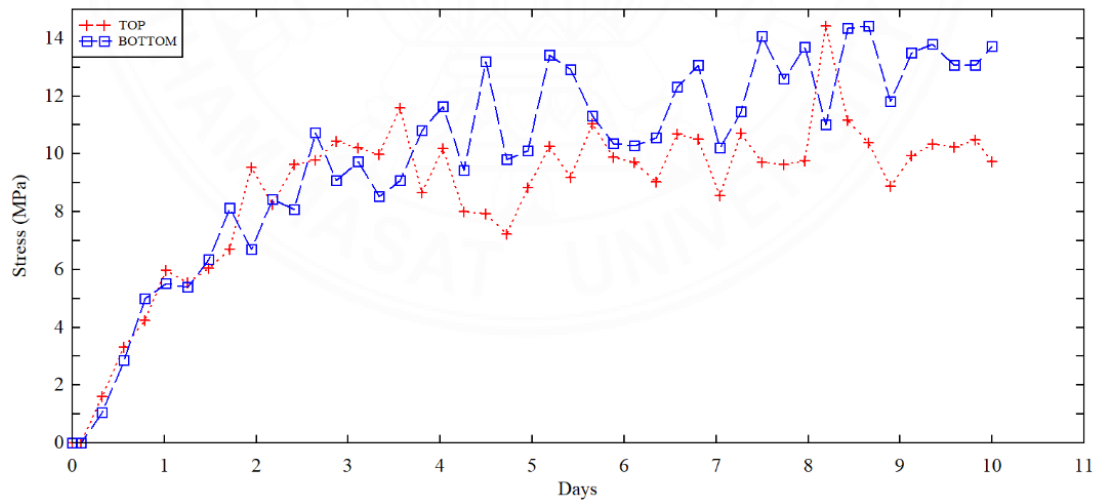
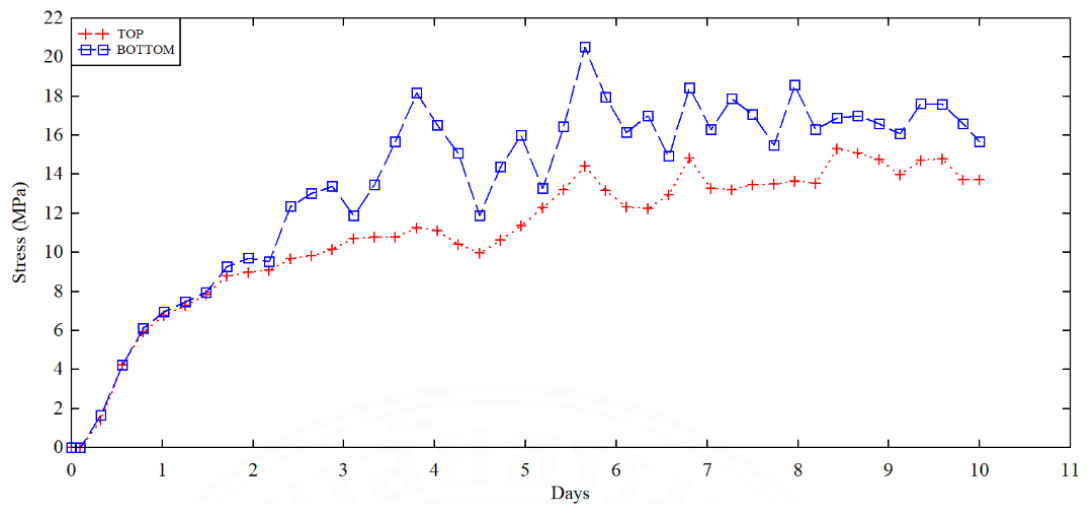


Figure 4.2 Highly mortar damaged location



(a) X axis



(b) Y axis

**Figure 4.3** Stress plots of the LFR tube

Similarly, the stress in the LFR sheet was also investigated. Therefore, the location where the sheet displays high stresses in the contours (see Figure 4.4) were selected to plot X- and Y- stresses to demonstrate the stresses (see Figure 4.5).

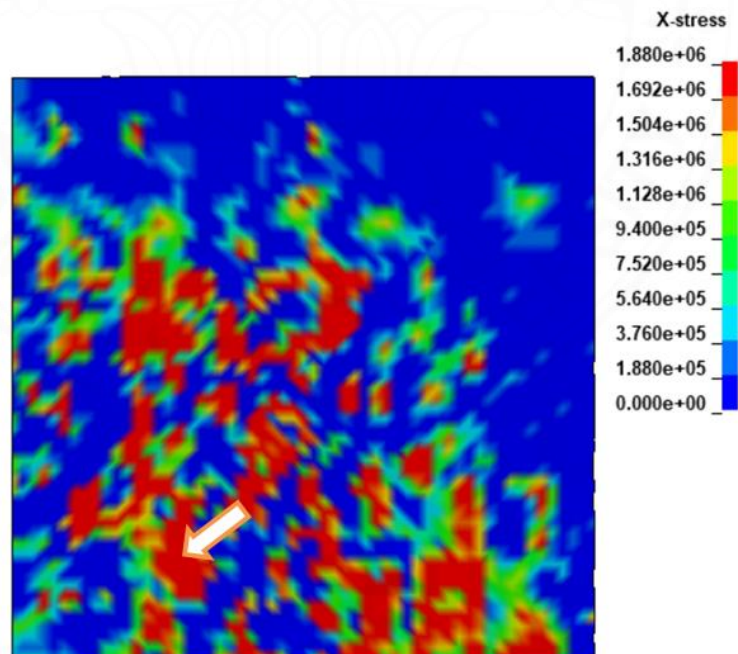


**Figure 4.4** Stress contour of LFR sheet

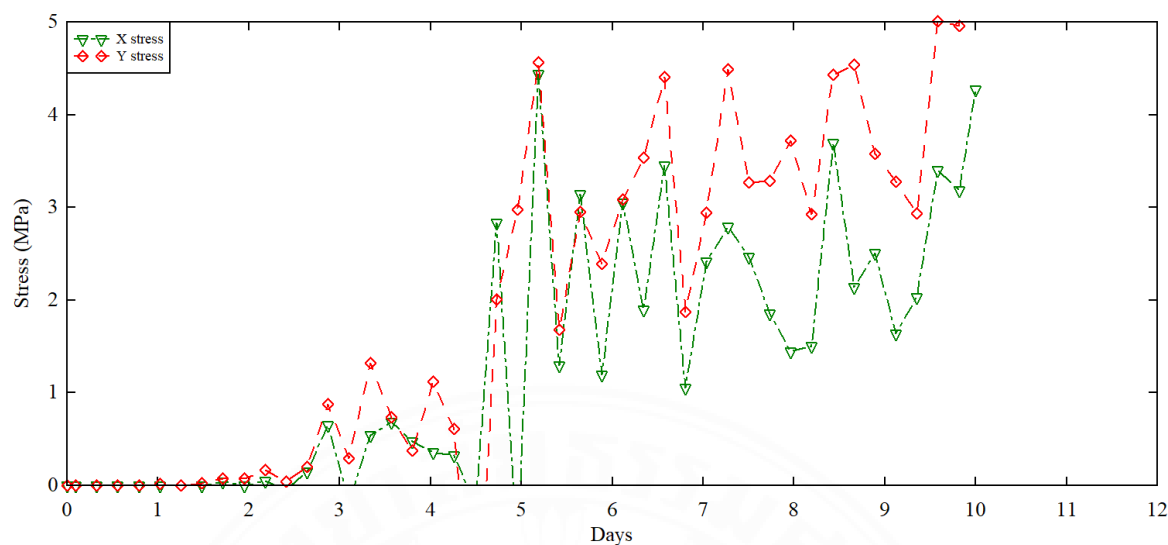


**Figure 4.5** Plots of X- and Y- stress in LFR sheet

### 4.3 Comparisons of field measurements with FE results from analysis case 1 and case 2

Several finite element analyses were performed to study the embankment settlements with LFR systems. For the convenience of presentation, the FEA results were presented in terms of the time (months) versus settlement (mm) and compared with their relevant field measurements. The long-term soil settlements of the embankments with  $1\text{m} \times 1\text{m}$  and  $2\text{m} \times 2\text{m}$  LFR systems from the FE results were compared with the field measurements as shown in Figure 4.6 and Error! Reference source not found. 4.7, respectively. Both field measurements and FEA results show that the spacing of the LFR mortar tube in the LFR system affects embankment settlement significantly.

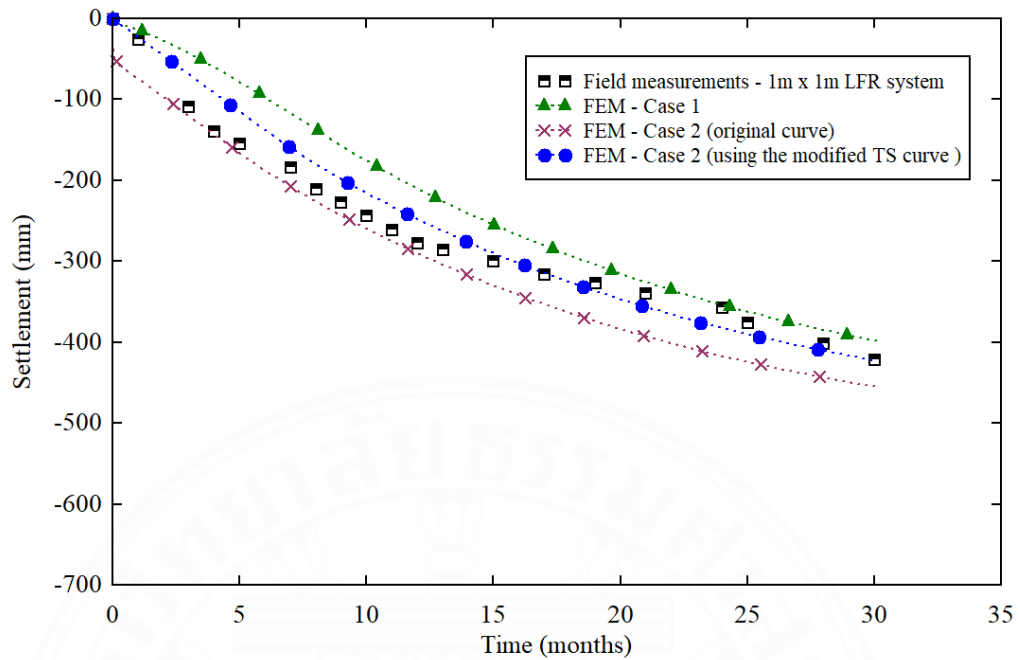


**Figure 4.6** Comparison of field measurement and FE results for 1m × 1m LFR system

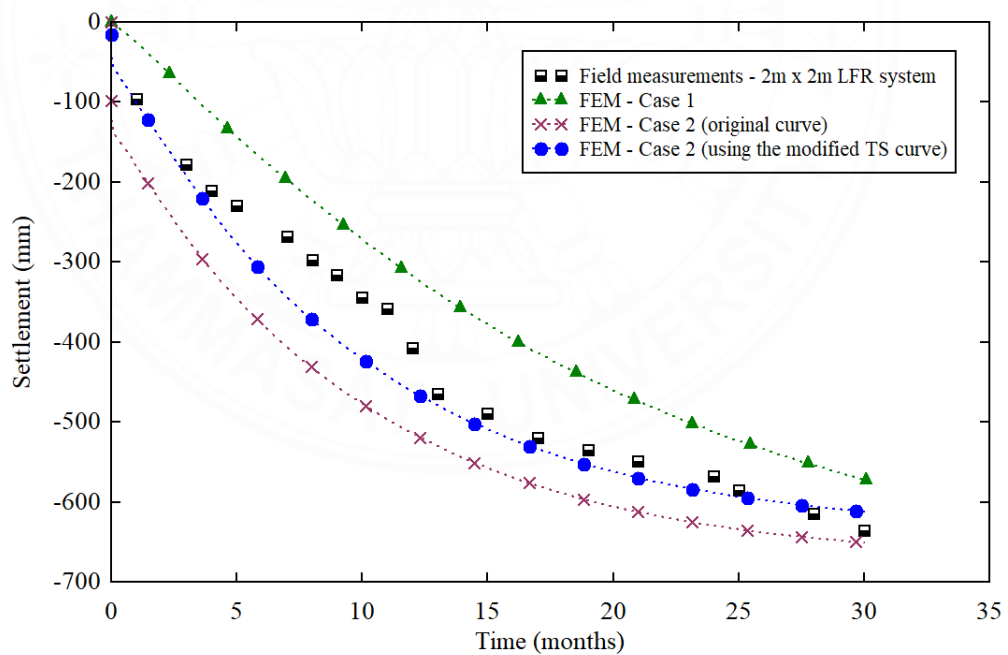


**Figure 4.7** Comparison of field measurement and FE results for 2m × 2m LFR system

The settlement from field measurements of 1m × 1m and 2m × 2m LFR systems were 421 mm and 636 mm at 30 months after the end of construction, respectively. FE

results from case 2 with the original stress strain curve reported the settlement of 455 mm and 650 mm for 1m × 1m and 2m × 2m LFR systems, respectively. While FE results from analysis case 2 which considers tension stiffening effects in the LFR mortar tube reported the settlement of 422 mm and 612 mm for 1m × 1m and 2m × 2m LFR systems, at the same period, respectively. The higher settlement resulted from case 2 – original curve is due to the absence of the injected mortar in the LFR system and the unenhanced stress- strain curve input to the LFR tube material card. Therefore, a higher settlement of the embankment can be expected as the LFR system excludes the stiffness contribution from the injected mortar. On the other hand, analysis case 1 shows a significant underestimation of the settlements in both 1m × 1m and 2m × 2m LFR systems compared to the field measurement due to the perfect bond assumption (see Table 4.1). It can be observed that the settlement rate (mm/month) was high and eventually becomes lower after the 12<sup>th</sup> month.

**Table 4.1** – Comparison of embankment settlements

	Settlement at 30 months (mm)			
	Field measurement	FE analysis case 1	FE analysis case 2 (original)	FE analysis case 2 (TS)
1m× 1m LFR system	421	398	455	422
2m × 2m LFR system	636	572	650	612

High stiffness achieved by the composite LFR mortar tube (case 1) results in low settlement. High stiffness was obtained as the contact between tube and mortar was defined as a contact with a perfect bond. This has deviated from the contact between tube and mortar in the actual LFR system. However, by employing the tension stiffening concept to the material model, integrating the contribution of the mortar into the tube in analysis case 2, stiffness of the tube was improved by the tension stiffening effects, and it revealed that the FEA results of case 2 were closer to the field



measurements. For case 2, the stress-strain curve of the tube was required to be modified so that effects of the bond between mortar and tubes, especially after mortar cracking, can be considered. This method provides a more realistic stiffness to the case 2 material card.

#### 4.4 Efficiency of the LFR system

Since there was no constructed embankment without the LFR system at the same site area for the real settlement measurement, therefore FE model of the embankment without the LFR system was analyzed by FEM to be used as the reference to demonstrate the efficiency of the constructed LFR system. The result of this model serves as free-soil settlement (embankment without LFR) and is used to compare with the field measurement of  $1\text{ m} \times 1\text{ m}$  and  $2\text{ m} \times 2\text{ m}$  LFR systems as shown in Figure 4.8. It can be seen that the LFR system with  $1\text{ m} \times 1\text{ m}$  tube spacing is very efficient to reduce embankment settlement compared to the  $2\text{ m} \times 2\text{ m}$  tube spacing model. The  $1\text{ m} \times 1\text{ m}$  and  $2\text{ m} \times 2\text{ m}$  LFR systems show 421 mm and 636 mm of settlement, respectively, compared to 710 mm of settlement from the embankment without the LFR system at 30 months.

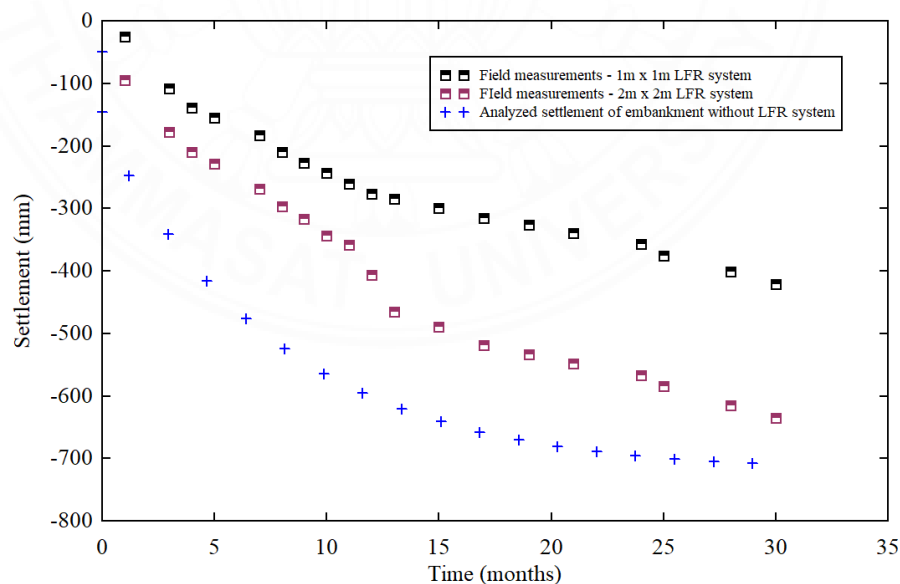


**Figure 4.8** Settlement of embankments with and without LFR system

The contours of the embankment settlement at the end of the 30<sup>th</sup> month are shown in Figure 4.9. The FEM without LFR system, the FEM with case 2 – TS curve LFR mortar tube (2m × 2m) system, and the FEM with case 2 – TS curve LFR mortar tube (1m × 1m) system, are shown in Figure 4.9 (a), (b), and (c), respectively.

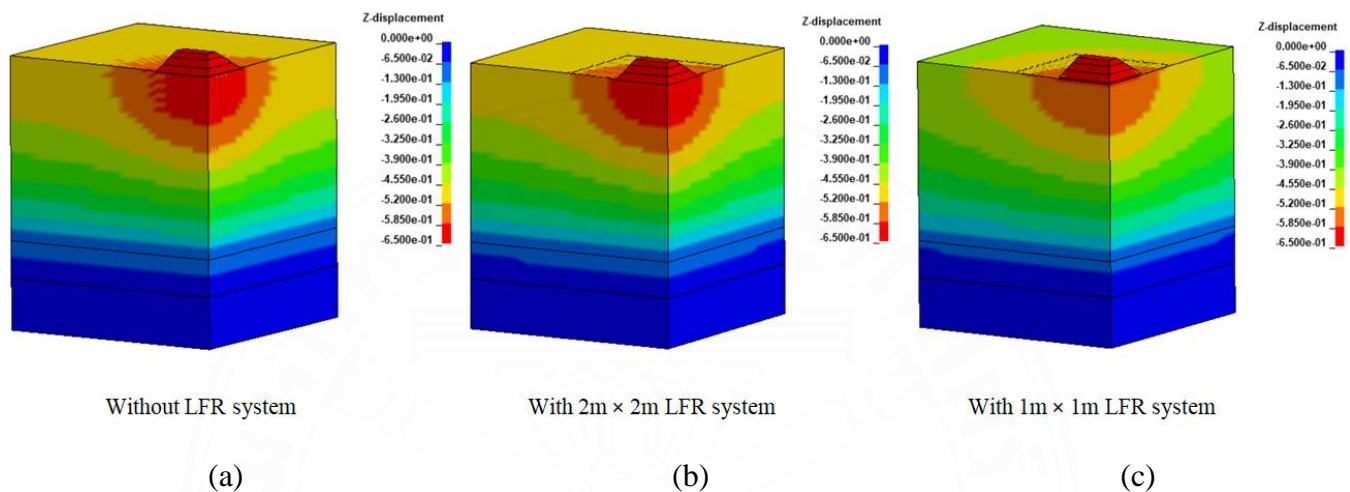


**Figure 4.9** Contour plots of the embankment settlements

#### 4.5 Rehabilitation of the rock embankment

The settlement of rock embankment is inevitable, but with the LFR system, the settlement rate can be lower. However, due to embankment settlement after several years upon construction, the effective height ( $H$ ) of the embankment as shown in Figure 4.10 can be reduced significantly (reduced to  $h$ ). Therefore, rehabilitation of the embankment will be required. Usually, rehabilitation adds more weight to the LFR system. However, the stresses in both the LFR sheet and LFR tube are much lower than their ultimate strength as previously explained in Section 3.1.6. Therefore, it is still possible to rehabilitate the existing rock embankment and extend the service life of the structure (see Figure 4.10).

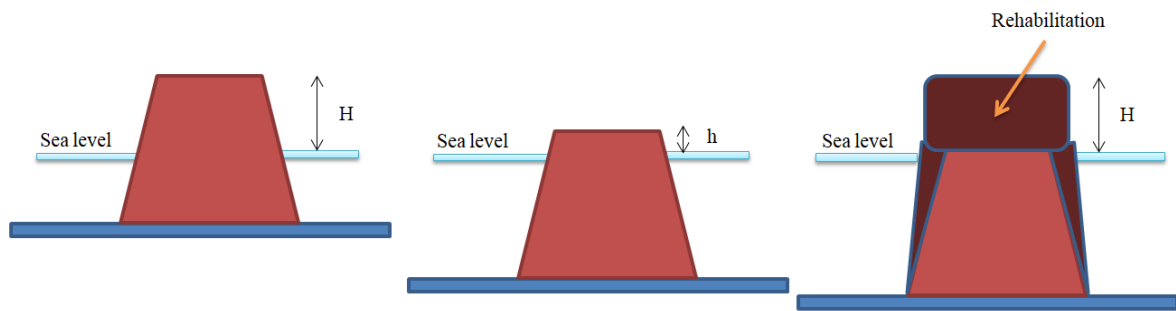


**Figure 4.10** Rehabilitated embankment



## CHAPTER 5

### CONCLUSIONS

The major findings of this study are summarized as follows:

1. The mechanism of the LFR system to decrease embankment settlement is by stretching of LFR mortar tube and LFR sheet. With tensile stiffness contributed from the LFR mortar tube, the embankment self-weight can be distributed to the entire area of the LFR system which is larger than the embankment base as well as by the tension carried by the LFR system. Therefore, soil pressure under the LFR system is significantly lower than that of the embankment without LFR system, resulting in less embankment settlement.
2. The injected mortar is used to keep the LFR tubes in shape and to provide better constructability. In addition, stiffness of cracked and uncracked mortar contributes to stiffness of the LFR mortar tube through bonding and tension stiffening effects.
3. FE results report tensile stress in LFR tube and sheet as well as tensile damage in mortar. This confirms that all the components of the LFR system are tension members. And the system works under stretched condition resulted from these tensile stresses.
4. LFR mortar tube demonstrates tension stiffening behavior similarly to behavior of RC members. With the tension stiffening effects included in the stress-strain curve of the LFR tube, the FE model can predict the long-term embankment settlement with satisfactory accuracy. On the other hand, the FE model which assumes perfect bonding by ignoring local slip between the cracked mortar and the LFR tube underestimates the embankment settlement.
5. Spacing of LFR tubes is one of the main design parameters for the LFR system. Both the real settlement measurement and the FE results show that the LFR system with  $1\text{m} \times 1\text{m}$  tube spacing shows a significant smaller embankment settlement compared to the system with  $2\text{m} \times 2\text{m}$  tube spacing.

6. Due to low stresses in LFR tube and LFR sheet, it is possible to rehabilitate the embankment by adding rocks on top of the existing rock embankment from time to time. Therefore, service life of the originally constructed embankment can be extended. This process will be economical because the service life of the embankment can be extended without having to demolish the existing embankment.



## REFERENCES

- Allam, S. M., Shoukry, M. S., Rashad, G. E., & Hassan, A. S. (2013). Evaluation of tension stiffening effect on the crack width calculation of flexural RC members. *Alexandria Engineering Journal*, 52(2), 163-173.
- A.S. Sahu (2014). Coastal Geosynthetics Protection an environmental appraisal. *Indian Journal of Spatial Science* (Vol. 5).
- ASTM, Assata M. "ASTM D3039-standard test method for tensile properties of polymer matrix composite materials." *Book ASTM D3039-standard test method for tensile properties of polymer matrix composite materials (ASTM International, 2017)*.
- Burkov, PV, Kalmykova, KG, Burkova, SP, & Do, TT (2014). Research of stress-deformed state of main gas-pipeline section in loose soil settlement. *In Proc IOP Conf.: Earth and Environmental Science*, (Vol. 21, No. 1, pp. 1-5).
- Gadpande, R.R. (2016). Analysis of piled Raft Foundation using ANSYS. *International Journal of Innovative Res. Sci. Technol*, 3, 142-146.
- G.G. Boldyrev, A. (2008). The Modeling of Deformation Process in Soils with Use of Ansys and Ls-Dyna Programs. *Sixth Internal Conference on Case Histories in Geotechnical Engineering*, VA.
- Huang, W., Fityus, S., Bishop, D., Smith, D., & Sheng, D. (2006). Finite- element parametric study of the consolidation behavior of a trial embankment on soft clay. *International Journal of Geomechanics*, 6(5), 328-341.
- Jiang, H., & Zhao, J. (2015). Calibration of the continuous surface cap model for concrete. *Finite Elements in Analysis and Design*, 97, 1-19.
- Likitlersuang, S., Chheng, C., Surarak, C., & Balasubramaniam, A. (2018). Strength and stiffness parameters of Bangkok clays for finite element analysis. *Geotechnical Engineering*, 49(2), 150-156

- Likitlersuang, S., Surarak, C., Wanatowski, D., Oh, E., & Balasubramaniam, A. (2013). Finite element analysis of a deep excavation: A case study from the Bangkok MRT. *Soils and foundations*, 53(5), 756-773.
- Massicotte, B., Elwi, A. E., & MacGregor, J. G. (1990). Tension-stiffening model for planar reinforced concrete members. *Journal of Structural Engineering*, 116(11), 3039-3058.
- Negahdar, A., Yadegari, S., & Houshmandi, S. (2016). Experimental study of the effect of stress level on time dependent deformation of sandy clay soil. *Japanese Geotechnical Society Special Publication*, 2(11), 457-460.
- Okamoto, M., Obara, T., Nakajima, Y., Yoshida, T., Kitamoto, Y., Kyokawa, H., Fujisaki, K. (2016). Effect of lattice-frame reinforced geosynthetics on seismic stability improvement of embankment on loose sand deposit. *Japanese Geotechnical Society Special Publication*, 2(68), 2324-2329.
- Okamoto, M., Yoshida, T., & Kitamoto, Y. (2009). Subgrade stabilization with lattice-frame-reinforced sheet. In *Proceedings of the 17th International Conference on Soil Mechanics and Geotechnical Engineering* (Vol. 1, 2, 3 and 4).
- Railway Technical Research Institute, 1992. *Standards for railway structures construction –earth structures– (in Japanese)*
- Saengsupavanich, C., Chonwattana, S., & Naimsampao, T. (2009). Coastal erosion through integrated management: A case of Southern Thailand. *Ocean & coastal management*, 52(6), 307-316.
- STS instruments company limited, Soil investigation report of site, Samut Sakhon, 2018.
- Surarak, C., Likitlersuang, S., Wanatowski, D., Balasubramaniam, A., Oh, E., & Guan, H. (2012). Stiffness and strength parameters for hardening soil model of soft and stiff Bangkok clays. *Soils and foundations*, 52(4), 682-697.
- Wagner, A. A. (1957). The use of the unified soil classification system by the bureau of reclamation. In *Proceedings of the 4th international conference on soil mechanics and foundation engineering, London*, (Vol. 1, No. 125, p. 553).
- Willford, M., Sturt, R., Huang, Y., Almufti, I., & Duan, X. (2010). Recent advances in nonlinear soil-structure interaction analysis using LS-DYNA. In *Proceedings of the NEA-SSI Workshop*, (pp. 6-8).

- Yoshida, T. et al., (2006). Effects of surface soil stabilization by a lattice-frame-reinforced sheet. In *Proc. 8th International Conference on Geosynthetics, Yokohama, 2006*.
- Zhang, L., Zhao, M., Shi, C., & Zhao, H. (2010). Bearing capacity of geocell reinforcement in embankment engineering. *Geotextiles and Geomembranes*, 28(5), 475-482.





## BIOGRAPHY

Name Mr. Isuru Tharanga Dias Rajakaruna Mohottige  
Education 2017: Bachelor of Engineering (Civil Engineering)  
Asian Institute of Technology

### Publications

I.T.Dias, G. Tanapornraweekit, S. Tangtermsirikul, 2020. Mechanism of Lattice Frame Reinforcement (LFR) System Used to Delay Settlement of Coastal Rock Embankments, *International Multi-Conference on Advance in Engineering, Technology, and Management (IMC-AETM2020)*, November 18-19, Bangkok, Thailand, p 159-164.

